scientific reports

Check for updates

OPEN

A DFT based insights for molecular designing of pyridine dipyrrolide core with benzodithiophene-based acceptors for organic solar cells

Mashal Khan[1,2,6], Ayesha Tariq[1,2,6], Iram Irshad[1,2], Muhammad Adnan Asghar[3]✉, Tansir Ahamad[4] & Ke Chen[5]✉

This study introduces a new series of organic compounds (PPH1–PPH8) derived from a pyridine dipyrrolide (PDP) core, aimed at enhancing the efficacy of organic solar cells. Their light absorption and charge transport capabilities were improved by altering the terminal groups of a reference molecule (PPHR) with strong electron-withdrawing units. The density functional theory (DFT) and time-dependent DFT (TD-DFT) calculations were employed at the M06/6-311G(d, p) level to examine the electronic and photovoltaic features of the designed chromophores. The findings indicated a notable redshift in the absorption spectra, broadening the absorption range from 562.874 to 617.913 *nm* accompanied by a substantial decrease in the energy gap from 2.677 to 2.468 *eV* in PPH1–PPH8. These results indicated enhanced solar light absorption due to end-capped modification. Moreover, these compounds demonstrated lower exciton binding energies (0.460–0.509 *eV*), signifying effective charge separation and improved exciton dissociation. Calculations of open-circuit voltage (V_{oc}), utilizing the standard acceptor ($PC_{71}BM$), further validated their photovoltaic potential. Electron-hole analysis identified PPH5 as a highly promising candidate, demonstrating significant spatial separation of charge carriers. Therefore, this research study presents a novel class of PDP-based chromophores with tailored optoelectronic characteristics, providing significant insights for the advancement of next-generation organic photovoltaic materials.

Keywords Pyridine dipyrrolide, Photovoltaic materials, Benzodithiophene acceptors, A – π – A, Open circuit voltage, DFT

To achieve clean energy *via* green technology based on organic molecules, the organic photovoltaics (OPV) are prominent class. They offer promising features such as low-cost, light-weight, non-toxic, large-area and flexible devices in contrast to their inorganic counterparts[1–3]. Further, the organic π-conjugated molecular systems are consistent in their symmetrical and intramolecular charge transfer (ICT) properties[4]. The basic functioning of an organic solar cell (OSC) consists of the absorption of a photon by an active material (usually donor); generation and diffusion of an exciton in donor; dissociation of exciton at the donor-acceptor interface which lead to formation of holes and electrons. Finally, the holes and electrons migrate towards the specific electrodes and their efficiency is greatly influenced by the insertion of different acceptor functionalities in an organic molecular structure[5].

Depending on the combination of specific donor and acceptor species, several types of OSCs are known such as the polymer-fullerene, single-junction OSC (single photoactive layer), multicomponent OSC (three or more components constitute a photoactive layer), polymer-small molecule and all-polymer and all-small molecule OSCs[6]. Currently, the single-junction OSCs are reported with the highest power conversion efficiency (PCE)

[1]Institute of Chemistry, Khwaja Fareed University of Engineering & Information Technology, Rahim Yar Khan 64200, Pakistan. [2]Centre for Theoretical and Computational Research, Khwaja Fareed University of Engineering & Information Technology, Rahim Yar Khan 64200, Pakistan. [3]Department of Chemistry, Division of Science and Technology, University of Education, Lahore, Pakistan. [4]Department of Chemistry, College of Science, King Saud University, Riyadh 11451, Saudi Arabia. [5]Department of Infectious Diseases, The Affiliated Hospital of Southwest Medical University, Luzhou 646000, China. [6]These authors contributed equally to this work: Mashal Khan and Ayesha Tariq. ✉email: adnan.muhammad@ue.edu.pk; chen_ke@swmu.edu.cn

of over 20% and photostability[7]. They effectively utilized non-fullerene acceptors (NFAs) and large band gap electron donors due to which they are well-known for being flexible, transparent and light-weight materials[8,9].

Pincer ligands were initially introduced in 1976 by Moulton and Shaw[10]. They have been successfully utilized in the formation of transition metal complexes. Pyridine dipyrrolide is an attractive pincer ligand which has garnered attention of scientists from several years due to its widespread use in the formation of well-defined complexes with early and late transition metals such as with Fe[11], Co, Cr[12], Zr[13], Mo[14], Zn[15], and Pd[16] etc. The free ligand i.e., $[pyrr_2Py]H_2$ is monomeric which has a coplanar structure owing to the orientation of incorporated pyrrole and pyridine moieties. The efficiency of this molecule can be enhanced by substituting robust end-capped acceptors in order to boost the photovoltaic and charge transfer properties. Hence, this research is highly based on the further exploration of this ligand.

The molecular engineering at terminal acceptors is an effective method for modulating the photovoltaic characteristics of organic chromophores. Literature indicates that the incorporation of benzothiophene (BT)-based acceptors with electron-withdrawing groups improves charge transfer towards the acceptor regions. This leads to increased short-circuit current (J_{sc}) and open-circuit voltage (V_{oc}) in the non-fullerene acceptors. The enhancement is chiefly attributable to the selective stabilization of the lower-lying LUMO, whereas the HOMO remains largely unaltered. Moreover, the absorption band is markedly expanded, hence contributing to the enhanced device performance[17].

At present, density functional theory has proven pivotal in elucidating the electrical and optical characteristics of NFA-OSCs. DFT simulations provide researchers with essential insights into molecular interactions, charge transport dynamics, and the energetics of innovative materials[18]. This computational approach facilitates the strategic design of high-efficiency non-fullerene acceptors (NFAs) and deepens the comprehension of the complex link between molecular architecture and device performance. Ultimately, these findings facilitate the advancement of next-generation high-performance organic solar cells[19,20]. In addition to HOMO/LUMO energy gaps, the DFT studies also interpret the non-covalent interactions (NCIs) in various organic molecules[21]. Researchers have synthesized vast variety of organic compounds accompanied by their DFT exploration, such as peptoids[22], chalchones[23], pepridone derivatives[24], pyrimidines[25], co-crystal salts[26,27], etc.

Considering the above-mentioned facts, herein, eight new A – π – A compounds (**PPH1- PPH8**) are designed from the reference (**PPHR**) which accommodate crystal core of pyridine dipyrrolide flanked with strong end-capped acceptors[28]. The research findings are presented here regarding their electronic, photophysical and photovoltaic properties *via* the DFT method which include interpretation of their FMOs, DOS, UV-Visible spectra, TDM, E_b and V_{oc} properties. It is anticipated that the proposed organic chromophores will provide revolutionary outcomes as unique photovoltaic materials.

Methodology

To investigate the quantum chemical properties of the entitled compounds (**PPHR** and **PPH1-PPH8**), Gaussian 09 program suite[29] at M06 level[30] with triple zeta i.e., 6-311G(d, p) basis set[31] was utilized. For this purpose, the studied compounds were optimized along with frequency analysis and found with minimum global energy without imaginary frequency. After this, various analyses such as the frontier molecular orbitals (FMOs), UV-Visible absorption, density of states (DOS), transition density matrix (TDM), open-circuit voltage (V_{oc}) and hole-electron were performed by using their optimized structures at the afore-mentioned functional. The exciton binding energy (E_b) was calculated using the FMOs and UV-Vis findings. The various software programs were employed for interpretation of data for these analyses which include the Avogadro[32], Origin 8.0[33], GaussSum[34], Multiwfn 3.7[35], PyMOlyze[36], and Chemcraft[37]. All the output files were visualized using the GaussView 6.0[38] software.

Results and discussion

In this study, $\mathbf{[pyrr_2Py]H_2}$ donor free ligand is chosen as the parent compound, which contains a pyridine dipyrrolide core. In order to avoid steric hindrance and computational cost, the upper toluene groups ($-C_6H_5CH_3$) are substituted with long alkyl chain groups ($-C_5H_{11}$) as represented in Fig. S1. After this structural modulation, the $\mathbf{[pyrr_2Py]H_2}$ is renamed as **PHHR** having A – π – A configuration. Further, eight different derivatives (**PPH1-PPH8**) are designed from the reference (**PPHR**) based on the pyridine dipyrrolide core and terminated with different strong benzothiophene based acceptors (A1-A8) which are displayed in Fig. 1. The aim of this research is to investigate their photovoltaic properties *via* the DFT and TD-DFT methods. Various parameters are analyzed which include the electronic, optical and photo-physical properties. Derivatives (**PPH4** and **PPH7**) have shown the most favorable results i.e., least energy gaps (2.468 and 2.491 *eV*, respectively) and highest absorption shifts (617.913 and 613.146 *nm*, respectively). The IUPAC names and structures of utilized benzothiophene based acceptors (A1-A8) are presented in the supplementary information (see Figure S2). However, the IUPAC names of reference and designed derivatives are mentioned in the Table S10. This DFT-based study explicates that the photovoltaic properties of organic compounds can be enhanced by their substitution with different end-capped acceptor units[39]. Their molecular structures are presented in the Figure S3, while their optimized geometries are shown in the Fig. 2. The Cartesian coordinates of studied chromophores are depicted in the Tables S1-S9.

Frontier molecular orbitals (FMOs) analysis

Frontier molecular orbitals analysis conceptualizes the chemical reactivity of molecules in terms of the interactions between their frontier orbitals[40]. It usually focuses on the highest occupied molecular orbital (HOMO) and the lowest unoccupied molecular orbital (LUMO) interactions. The HOMO is logically viewed as electron donating or valence band, while the LUMO is electron accepting or conduction band[41,42]. For an

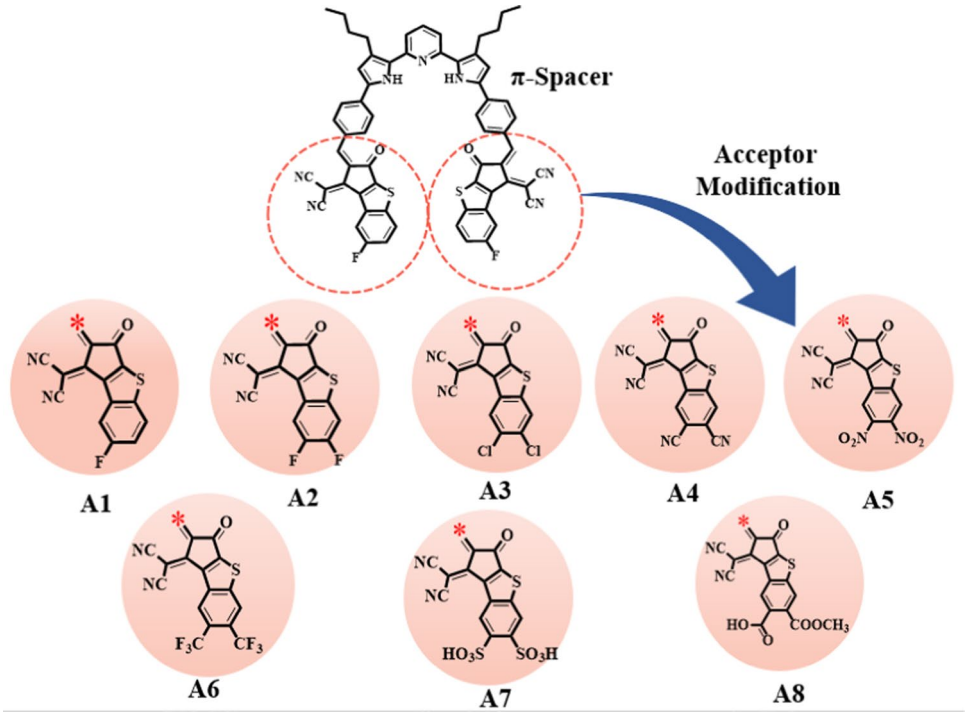

Fig. 1. Schematic representation of the designed compounds.

effective charge transfer within a molecule, electron density must be shifted promptly from the HOMO towards the LUMO[43]. The difference in energies of HOMO and LUMO deliberately elucidates the chemical reactivity[44], stability[45], and intramolecular charge transfer[46]. Overall, the FMOs analysis estimates the electronic properties of organic chromophores[47]. Therefore, this analysis is performed for the titled molecules (**PPHR** and **PPH1-PPH8**) at M06/6-311G(d, p) level and the results are tabulated in the Table 1. It represents the energies of major orbitals (HOMO and LUMO) along with their energy gaps (E_{gap}). Similarly, results for other orbitals (HOMO-1/LUMO + 1 and HOMO-2/LUMO + 2) are presented in the Table S11 and Figure S4).

The computed energies (E_{HOMO} and E_{LUMO}) for reference compound (**PPHR**) i.e. −5.318 and − 1.227 *eV*, respectively, are higher than other derivatives (**PPH1-PPH8**). Similarly, the energy gap for **PPHR** is found as 4.091 *eV* which is much higher than designed chromophores. Moreover, the Table 1 shows that, among **PPH1-PPH8** systems, the compounds (**PPH4** and **PPH7**) show the least energy gaps (2.468 and 2.491 *eV*) which might be due to the accommodation of 1-(dicyanomethylene)−2-methylene-3-oxo-2,3-dihydro-1-*H*-benzo[b]cyclopenta[d]thiophene-6,7-dicarbonitrile and 1-(dicyanomethylene)−2-methylene-3-oxo-2,3-dihydro-1-*H*-benzo[b]cyclopenta[d]thiophene-6,7-disulfonic acid as the terminal acceptors, respectively. According to literature analysis, the presence of strong electron acceptors over the terminals significantly reduces the energy gap[39,40]. In case of the above-mentioned acceptors, –CN and $–SO_3H$ groups are present which lower the overall energy gaps of respective compounds. The following decreasing order of E_{gap} is observed for the investigated compounds in *eV*: **PPHR > PPH1 > PPH8 > PPH2 > PPH3 > PPH6 > PPH5 > PPH7 > PPH4**.

The FMOs contour surface diagrams for the entitled molecules are displayed in the Fig. 3 which represent the electronic cloud distribution with blue and red regions showing positive and negative intensities, respectively. In HOMO of **PPHR** compound, the electron density is observed over the whole molecule except nitrogen and *n*-butyl chain. While, in LUMO, it spreads over the entire molecule except *n*-butyl chain. Similarly, in HOMO of derivatives (**PPH1-PPH8**), the electron density lies over the π-linker units, while in their LUMO, the clouds are seen over the terminal acceptors. Hence, the analyzed molecular systems show significant charge transfer from the π − spacer towards the acceptor regions. Concluding this discussion, it is inferred that the designed chromophores have emerged as efficient optoelectronic materials.

UV-Visible analysis

The UV-Visible analysis elucidates the charge transmission properties in the studied chromophores[41,42]. There are several parameters among which the absorption maxima (λ_{max}) and excitation energy (E) are the most significant. They refer to the exact energy necessary for a transition to occur and the oscillation frequency (f_{os}) represents the possibility of transition[48]. Hence, a compound with broader absorption attains higher λ_{max} and f_{os} while, lower E values. The broader absorption further leads to efficient intramolecular charge transfer[49]. The UV-Visible analysis is performed using the time-dependent DFT (TD-DFT) at selected level in both gas and chloroform solvent. The analysis includes the interpretation of λ_{max}, f_{os}, E and excited state transitions up to six energy levels. The representative values are displayed in the Table 2. However, other results are tabulated in the Tables S12 and S13. The graphical representation of the absorption spectra is plotted in the Fig. 4.

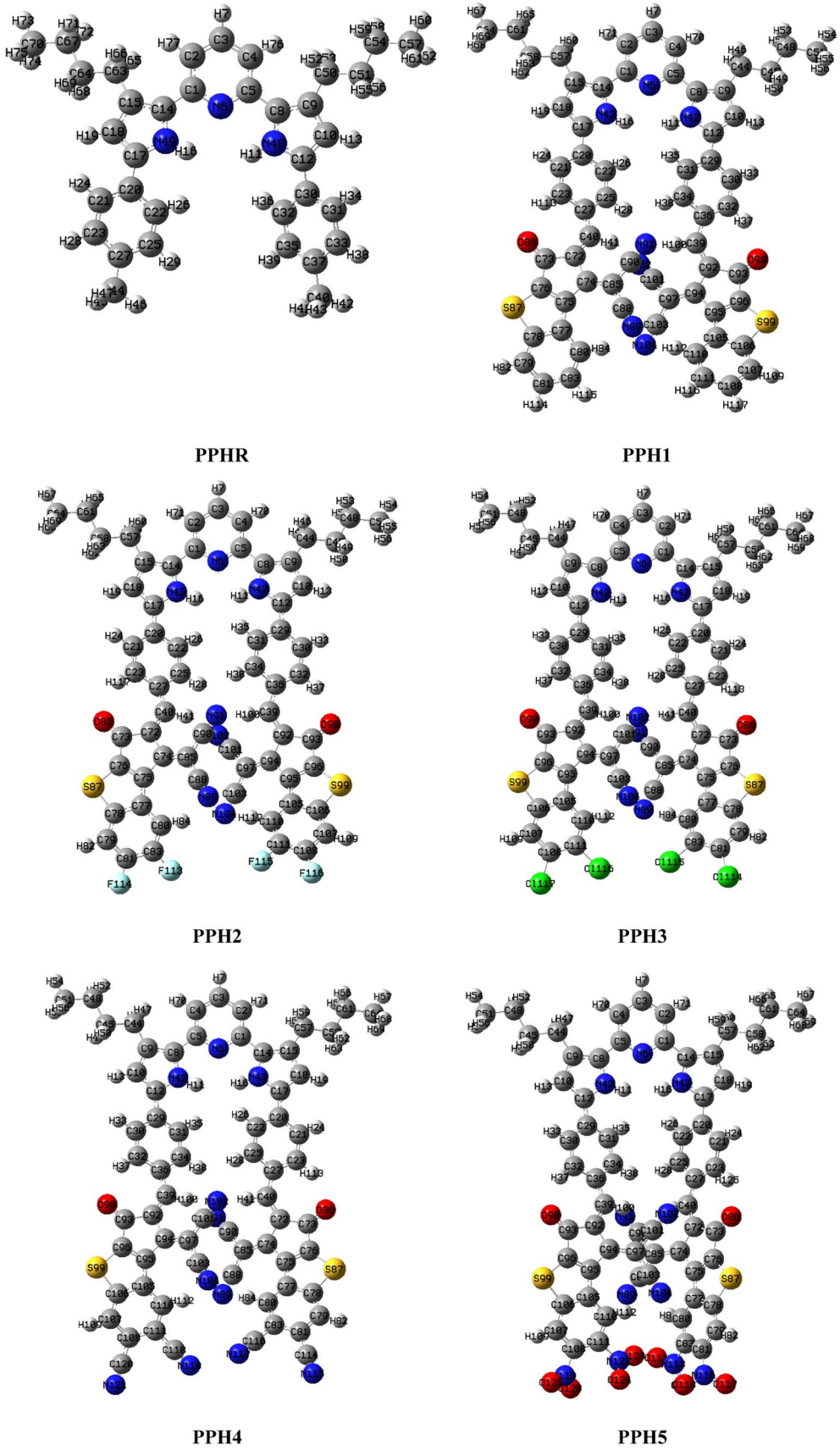

Fig. 2. Optimized structures of the investigated chromophores (**PPHR** and **PPH1-PPH8**).

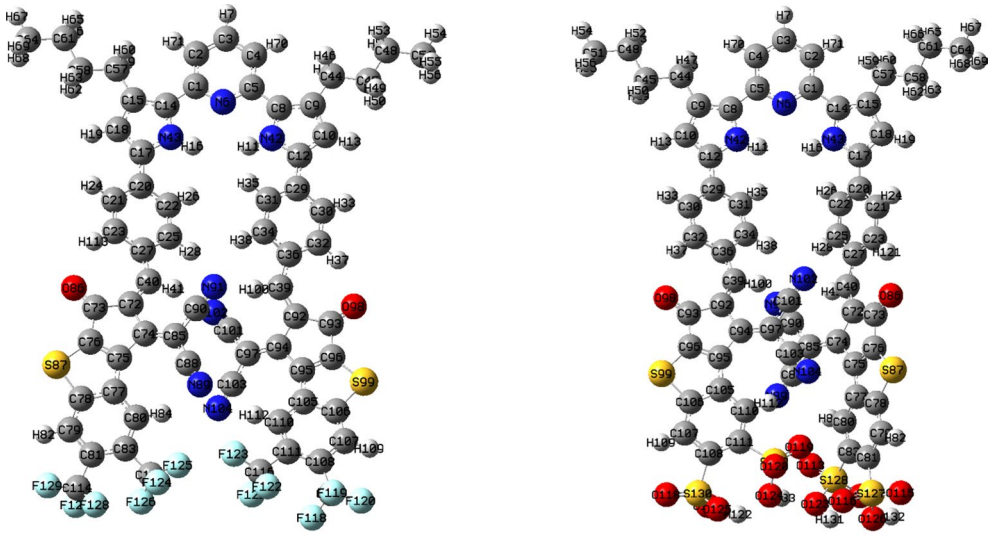

PPH6 **PPH7**

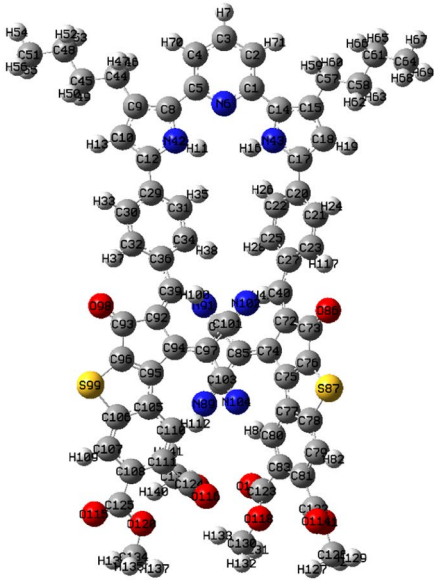

PPH8

Fig. 2. (continued)

The data show that in gas phase, all the designed derivatives (**PPH1-PPH8**) exhibit significantly higher λ_{max} values in a range of 562.874-617.913 *nm* as compared to the reference (**PPHR**) i.e., 384.114 *nm*. The following decreasing order for λ_{max} is observed in these compounds: **PPH4** (617.913) > **PPH7** (613.146) > **PPH5** (603.153) > **PPH6** (593.339) > **PPH3** (585.688) > **PPH2** (580.532) > **PPH8** (576.135) > **PPH1** (562.874) > **PPHR** (384.114) in *nm*. Conversely, they show lower transition energies (*E*) in a range of 2.007–3.228 *eV*. The following pattern is observed for *E* among the investigated chromophores: **PPH4** (2.007) < **PPH7** (2.022) < **PPH5** (2.056) < **PPH6** (2.090) < **PPH3** (2.117) < **PPH2** (2.136) < **PPH8** (2.152) < **PPH1** (2.203) < **PPHR** (3.228) in *eV*. The oscillation frequency (f_{os}) are observed as **PPHR** (0.406), **PPH1** (0.089), **PPH2** (0.077), **PPH3** (0.068), **PPH4** (0.033), **PPH5** (0.011), **PPH6** (0.048), **PPH7** (0.030) and **PPH8** (0.029). Lastly, the molecular orbital contributions observed for **PPHR** and **PPH1-PPH8** are H→L (97%), H→L (92%), H→L (93%), H→L (93%), H→L (94%), H→L (33%), H→L (94%), H→L (70%) and H→L (82%), respectively. **PPH4** and **PPH7** compounds show the most red-shifted absorption values (617.913 and 613.146 *nm*) which is due to the presence of strongly electron-withdrawing species in their acceptors (–CN and $–SO_3H$ groups, respectively). The molecular orbital transitions responsible for this red-shift are the first excited state transitions from HOMO to LUMO represented as H→L (94%) and H→L (70%) respectively. The reason behind this red-shift is principally due to the enhanced electron-withdrawing capacity of the terminal acceptors, which substantially stabilize the LUMO energy levels.

Compounds	E_{HOMO}	E_{LUMO}	E_{gap}
PPHR	−5.318	−1.227	4.091
PPH1	−5.743	−3.066	2.677
PPH2	−5.843	−3.238	2.605
PPH3	−5.871	−3.281	2.590
PPH4	−6.105	−3.637	2.468
PPH5	−6.107	−3.564	2.543
PPH6	−5.973	−3.423	2.550
PPH7	−6.051	−3.560	2.491
PPH8	−5.869	−3.208	2.661

Table 1. Assessments of energy gaps for the **PPHR** and **PPH1-PPH8** compounds.

This leads to a diminished HOMO-LUMO energy gap in **PPH4** and **PPH7** (2.468 and 2.491 *eV*, respectively) which facilitates the ICT, as indicated by the predominant transitions accounting for over H→L (90%) of the low-energy absorption bands.

Similarly, in case of the chloroform solvent, the compound (**PPH4**) shows the utmost $\lambda_{max} = 550.258$ *nm* with correspondingly least transition energy as 2.253 *eV*. Overall, the absorption values of derivatives in this case are lesser than gaseous phase values and following trend is observed: **PPH4** (550.258) > **PPH5** (540.943) > **PPH7** (533.265) > **PPH6** (528.853) > **PPH8** (526.048) > **PPH3** (502.469) > **PPH2** (496.195) > **PPH1** (487.685) > **PPHR** (340.672) in *nm*. Therefore, it is anticipated that the studied chromophores exhibit significant photonic properties with broader absorptions in the visible region and lower excitation energies[50].

Density of States (DOS)

Density of states analysis is used to evaluate the electronic structure of a molecular system by examining the contribution of electronic states at specific energy levels[51,52]. This analysis provides a comprehensive view of the energy distribution and helps in calculating the E_{gap} between the HOMO and LUMO[53]. By complementing the FMOs analysis, DOS calculations offer insights into how different fragments within a molecule contribute to the overall electronic structure which often aids in understanding their electronic properties and behavior[54]. To examine the ICT, the designed chromophores are categorized into two fragments: the π-spacer (core unit) and the acceptor (end-capped group). In the DOS spectra for **PPHR** and its derivatives (**PPH1**-**PPH6**), the π-bridge and acceptor contributions are shown by green and red curves, respectively, while the black curve represents the combined contribution of both fragments, as depicted in the Fig. 5.

In these DOS plots, the valence band (HOMO) is denoted on the left side, and the conduction band (LUMO) on the right side over the x-axis. The energy gap, which is the distance among the HOMO (H) and LUMO (L) foremost peaks is also illustrated in the Fig. 5. In HOMO, the electronic contributions for the π-spacer are examined as 80.0, 91.3, 91.4, 91.3, 91.6, 91.3, 91.9, 91.2 and 91.1% in **PPHR-PPH8**, respectively. Whereas, for LUMO, this charge density is investigated as 78.5, 7.7, 7.1, 6.2, 3.8, 7.6, 4.9, 7.4 and 16.4%, respectively. Likewise, for acceptor moieties, the electronic contributions are 20.0, 8.7, 8.6, 8.7, 8.4, 7.7, 8.1, 7.8 and 7.9% in HOMO, accordingly. While, for the LUMO, 21.5, 92.3, 92.9, 93.8, 96.2, 92.4, 95.1, 92.6 and 83.6% charge contributions are noted for **PPHR-PPH8**, respectively (see Table S14). Furthermore, the DOS maps reveal that the maximum charge density for the HOMO is concentrated on the π-spacer, marked by a green peak around − 7.8 *eV*. Similarly, the charge density for the LUMO is indicated by red peak between − 3 to −3.5 *eV*, demonstrating charge transfer from the central core towards the acceptors. Thus, the DOS graphs strongly support the FMOs pictographs showing that there is a considerable delocalization of the electronic cloud and substantial charge transfer from the central core to the acceptor groups.

Non-Covalent interactions (NCI)

Non-covalent interaction analysis functions as a comprehensive evaluation technique to elucidate weaker molecular interactions, encompassing hydrogen bonding, Van der Waals forces and steric effects[55]. Such interactions in the organic molecules predict their chemical reactivity and stability characteristics.

Multiwfn software is employed to produce the 2D reduced density gradient (RDG) scatter plots and the color-filled RDG isosurfaces for all the investigated compounds (**PPHR** and **PPH1**-**PPH8**) are visualized using the VMD software (see Fig. 6). RDG plot is drawn between $(\lambda_2)\rho$ on the x-axis and RDG values on the y-axis in *a.u.* The type of interactions is distinguished as bonded ($\lambda_2 < 0$) and non-bonded ($\lambda_2 > 0$) interactions on the x-axis. The RDG in conjunction with electron density in NCI analysis produces visual representations that illustrate attractive forces in blue, weaker Van der Waals interactions in green, and steric repulsions in red[56].

The NCI study demonstrates varying impacts of different substituents on the interaction behaviors of the studied compounds. The sign of the $(\lambda_2)\rho$ function mapping reveals essential information regarding the nature and strength of interactions. The blue patches in the NCI plot signify robust attractive interactions, typically indicative of hydrogen bond production. These fundamental atomic interactions greatly enhance molecule stability and intra- or intermolecular structural connectivity. The high intensity and extensive distribution of blue regions within these areas indicate the presence of well-defined hydrogen bonding in these structures that increase stiffness.

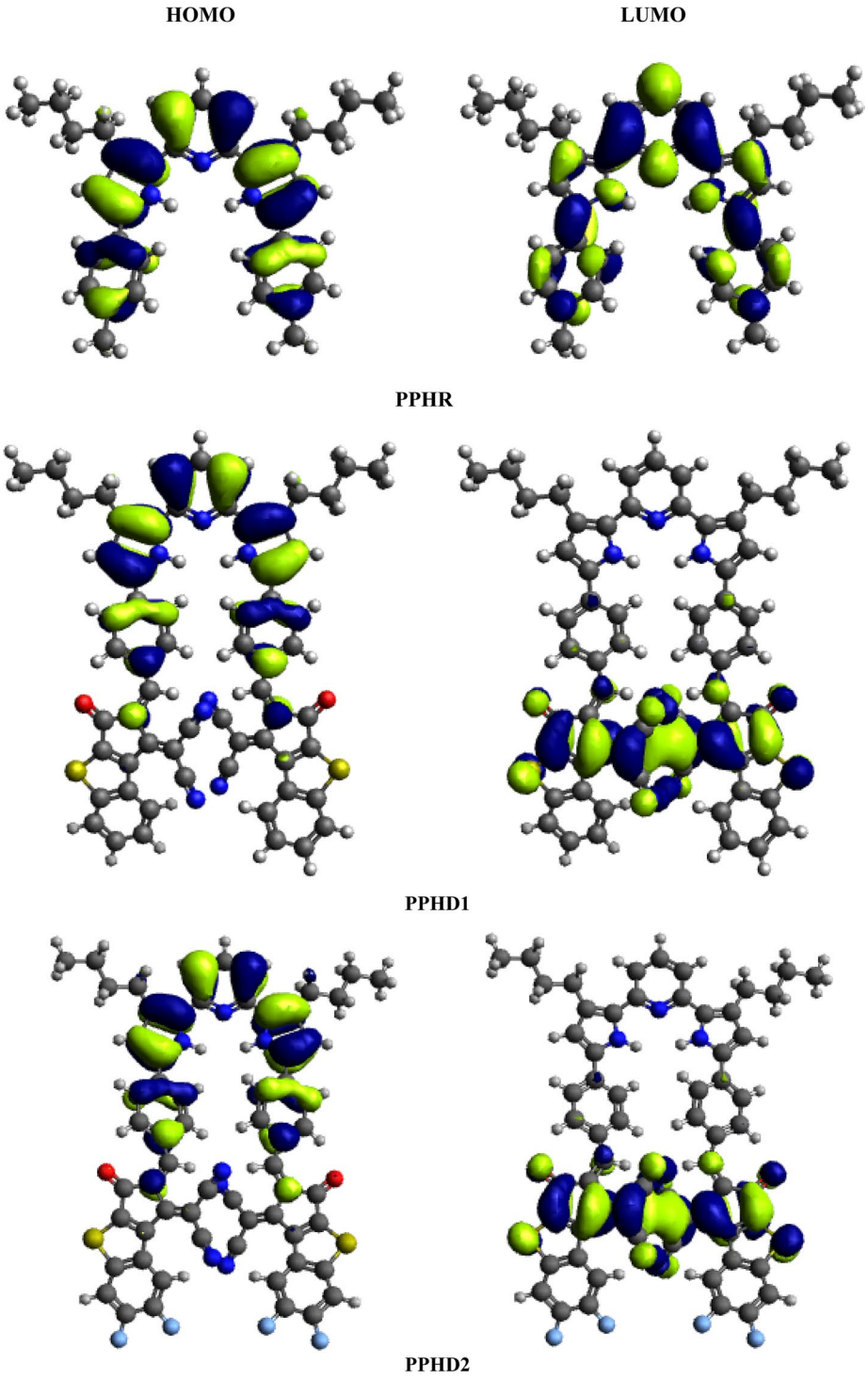

Fig. 3. HOMOs and LUMOs of the entitled compounds.

Overall, this study illustrates how molecular forces equilibrate between attraction and repulsion to sustain intermolecular interactions. Molecular stability arises from robust hydrogen bonding and secondary Van der Waals interactions; however, the structural constraints are imposed by steric repulsion.

Transition density matrix (TDM)

The transition density matrix is an essential tool for assessing charge transitions within a molecule[57]. It provides insights into the distribution of electrons and holes, as well as the rate of charge transfer and the nature of excited states[58]. In a TDM plot, two significant regions need to be considered: the diagonal and off-diagonal areas. The diagonal elements correspond to the excited states of molecule, while the off-diagonal elements indicate charge

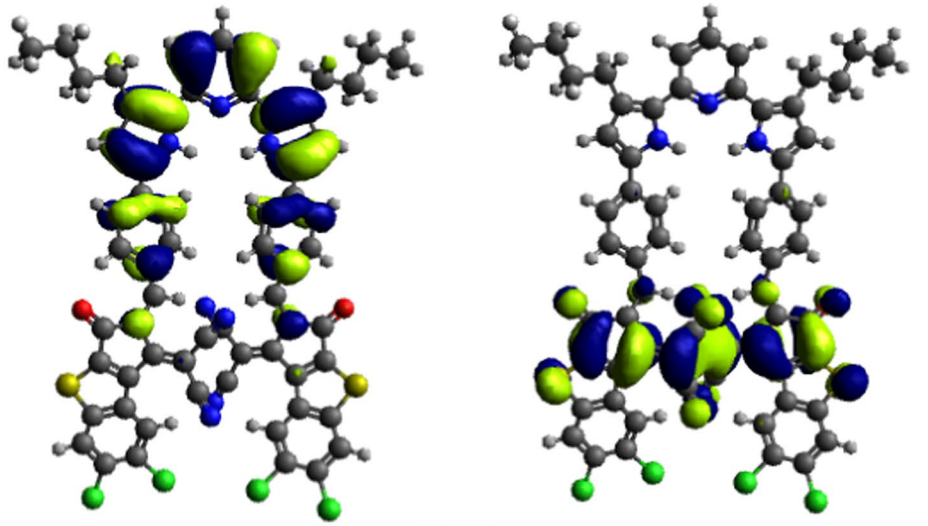

PPHD3

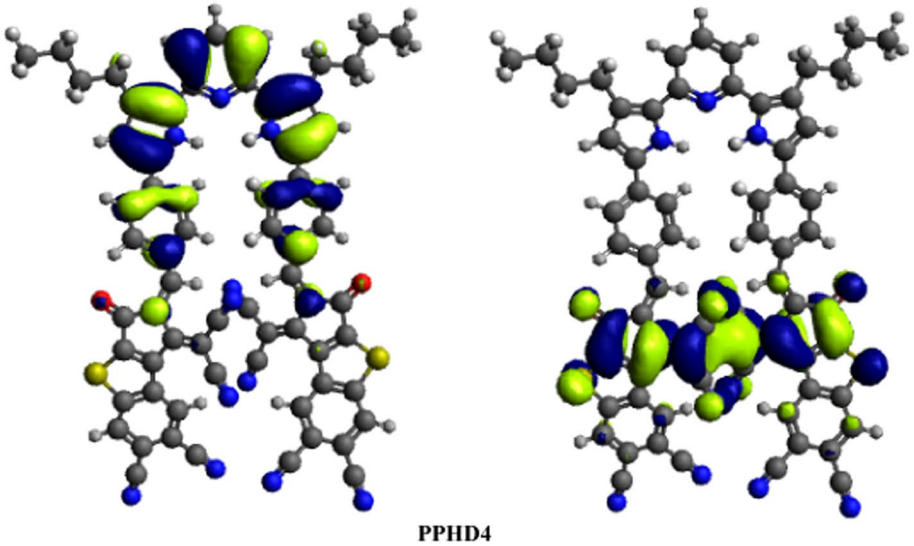

PPHD4

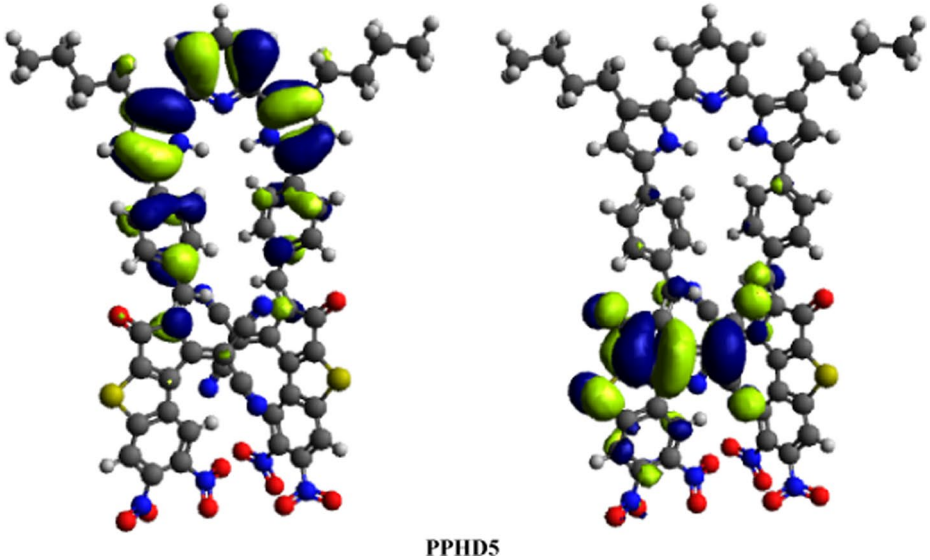

PPHD5

Fig. 3. (continued)

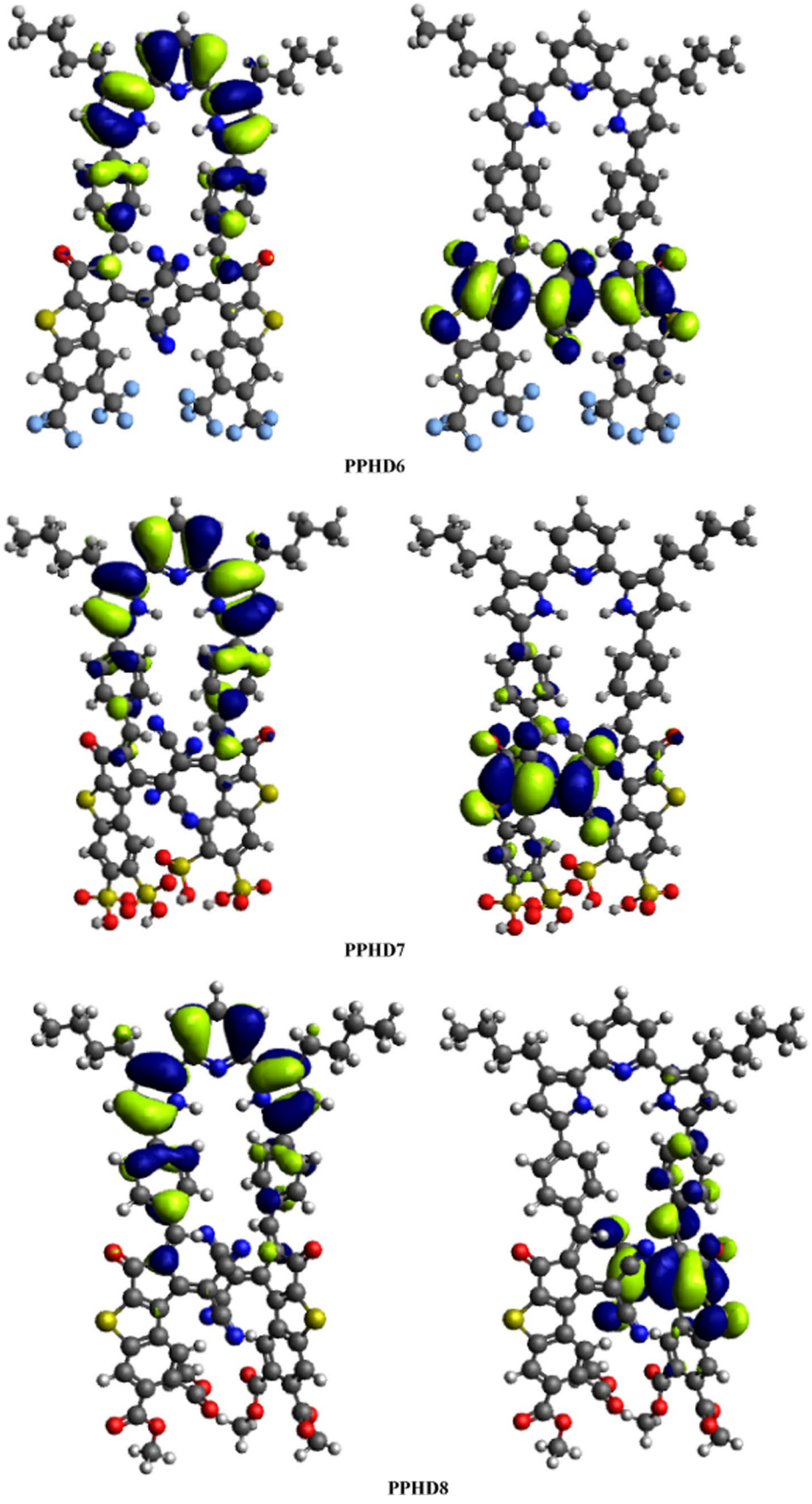

Fig. 3. (continued)

	System	TD-DFT λ_{max} (nm)	E (eV)	f_{os}	MO Contributions
[a]Phase	**PPHR**	384.114	3.228	0.406	H→L (97%)
	PPH1	562.874	2.203	0.089	H→L (92%)
	PPH2	580.532	2.136	0.077	H→L (93%)
	PPH3	585.688	2.117	0.068	H→L (93%)
	PPH4	617.913	2.007	0.033	H→L (94%)
	PPH5	603.153	2.056	0.011	H→L (33%)
	PPH6	593.339	2.090	0.048	H→L (94%)
	PPH7	613.146	2.022	0.030	H→L (70%)
	PPH8	576.135	2.152	0.029	H→L (82%)
[b]Phase	**PPHR**	340.672	3.639	0.639	H→L + 1 (96%)
	PPH1	487.685	2.542	1.163	H-1→L + 1 (71%)
	PPH2	496.195	2.499	1.245	H-1→L + 1 (63%)
	PPH3	502.469	2.468	1.190	H-1→L + 1 (63%)
	PPH4	550.258	2.253	1.160	H→L + 3 (93%)
	PPH5	540.943	2.292	0.375	H-1→L (48%)
	PPH6	528.853	2.344	1.099	H→L + 3 (91%)
	PPH7	533.265	2.325	0.894	H-1→L + 1 (79%)
	PPH8	526.048	2.357	0.833	H→L + 2 (46%)

Table 2. Wavelength (λ_{max}), excitation energy (E), oscillator strength (f_{os}) and molecular orbital contributions of compounds (**CBR** and **CBD1-CBD8**) in gaseous and solvent phases. [a]Gaseous Phase, [b]Chloroform Solvent.

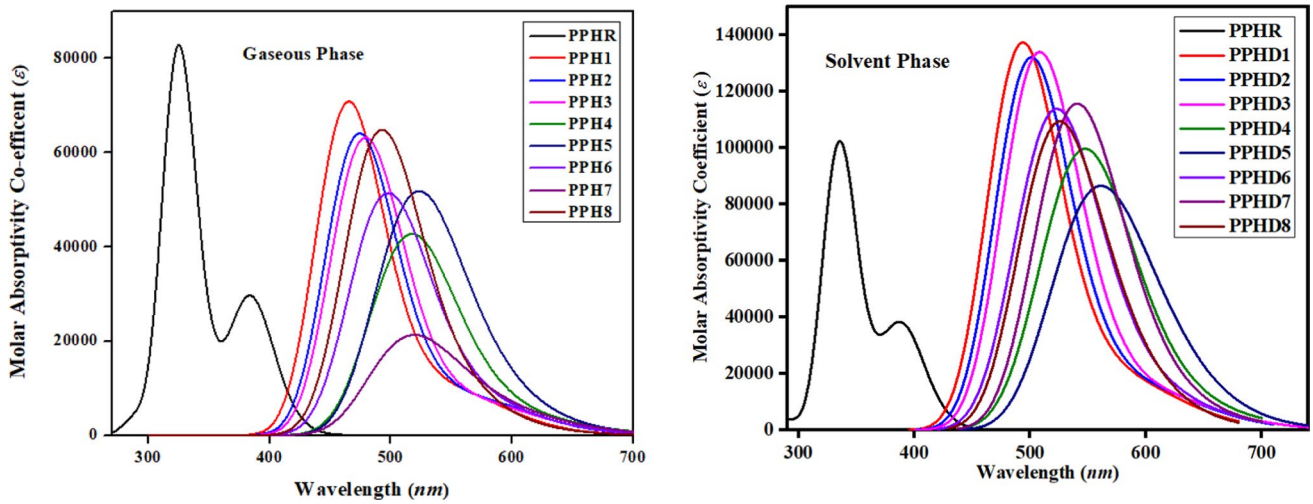

Fig. 4. UV-Visible spectra for the entitled compounds in gas and chloroform solvent.

transfer processes[59]. The TDM map of each chromophore separates different fragments (π-linker and terminal acceptor) with the help of horizontal and vertical colored lines offering a detailed view of charge coherence and hole-electron localization in diagonal and off-diagonal regions. Moreover, the brighter sections of TDM plots are enclosed in a ring showing the prominent sections of charge localization (see Fig. 7). Due to very less contribution of H-atoms in these transitions, they are excluded in this analysis[60]. The atom numbers of each individual molecule are plotted on the x- and y-axes[61]. Figure 7 shows that bright patches are consistently present both diagonally and off-diagonally in the acceptor and π-linker regions, illustrating efficient charge transfer within a molecule. Moreover, these bright regions also signify the presence of excited states in the TDM plots. The TDM heat maps for these chromophores indicate efficient charge transfer, without charge coherence being trapped. These heat maps are influential in the development of solar cells, as they suggest a smoother and more efficient flow of electrons from the central core towards the end-capped acceptor groups.

Hole-Electron analysis

A heat map is a visual illustration for analyzing hole-electron interactions in photovoltaic materials, offering insight into the spatial and temporal behavior of charge carriers[62]. It provides crucial information about the function of each fragment in generating holes and electrons. Additionally, it helps evaluate how much overlap

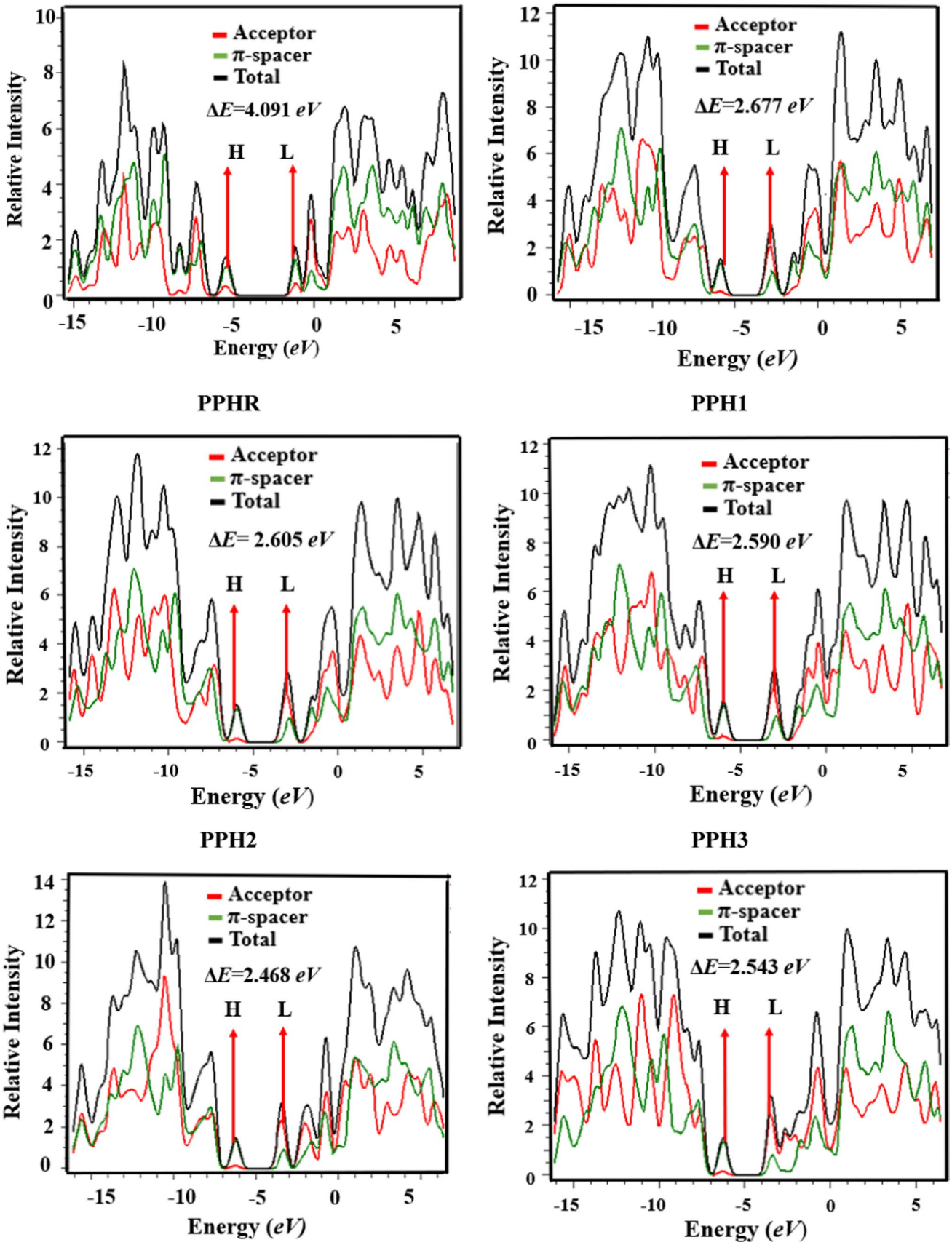

Fig. 5. DOS spectra of the studied compounds (**PPHR** and **PPH1-PPH8**).

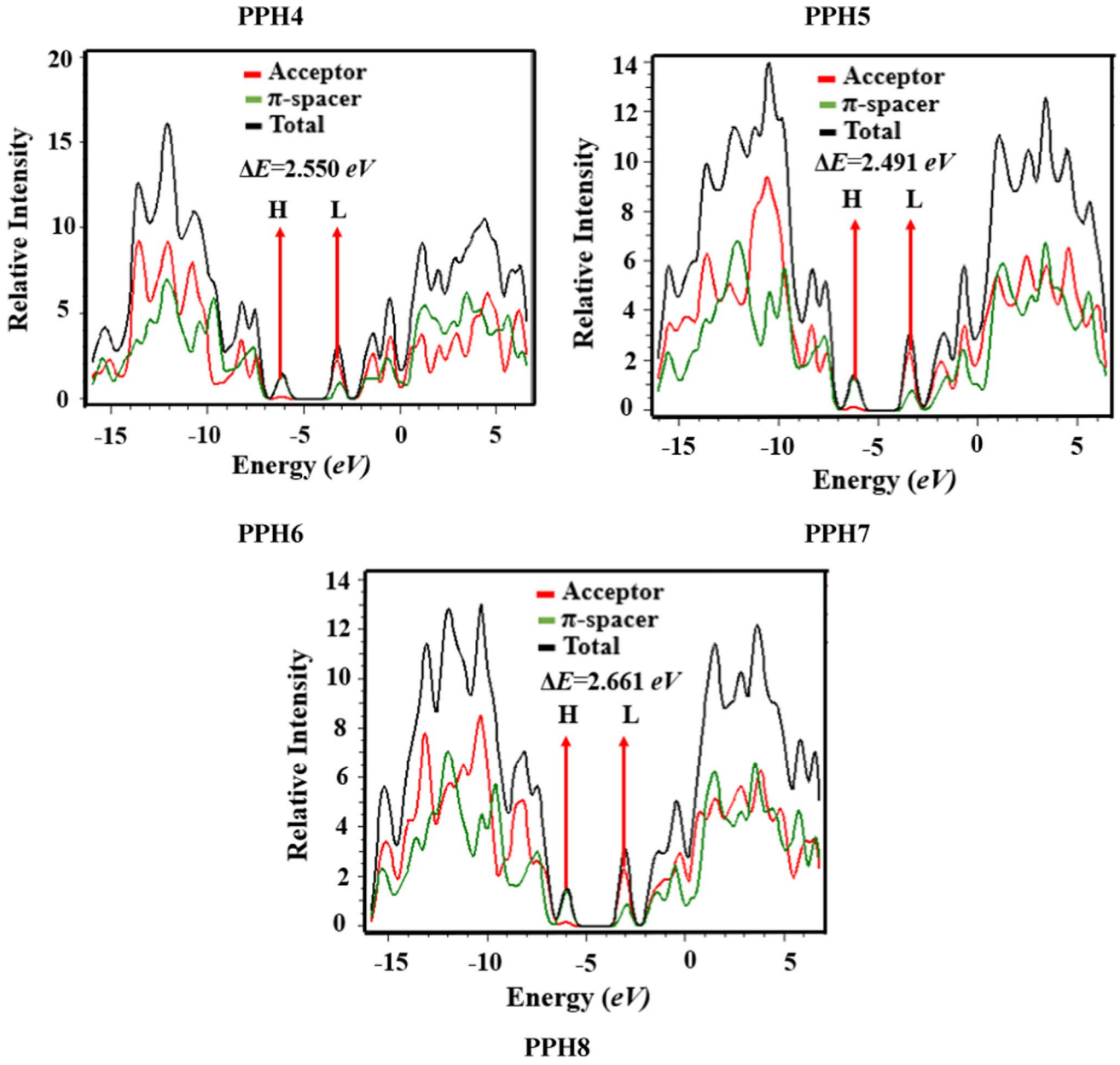

Fig. 5. (continued)

exists between holes and electrons within the photoactive layer of OSCs[63]. In this study, Multiwfn 3.8 is employed to analyze electron-hole interactions and determine the charge movement within the examined molecules.

From Fig. 8, it is observed that in the reference molecule (**PPHR**) and designed compounds (**PPH1-PPH3**), hole is generated at the carbon atoms (C7 and C11) of benzene and pyridine ring of π-spacer and electron intensity is also found concentrated over the C-atom of benzene and thiophene rings. In **PPH5-PPH7** compounds, the band displays a moderate density, while the hole band achieves a maximum intensity similar to that of the previously designed chromophores. However, in **PPH4** and **PPH8**, a slight hole density is concentrated around the C9, C10 and C27 atoms within the π-spacer, whereas the electron density is predominantly found at C41 and O51 atoms within the 2-(4-oxocyclopent-2-en-1-ylidene)malononitrile segment of the acceptor. Significantly, all visual representations reveal that the hole predominantly forms within the π-linker segment at the carbon atoms, whereas the electron density peaks are found notably across different atomic sites in the acceptor regions. Each chromophore displays notable electron and hole clouds across different parts of the molecule. **PPH4** and **PPH8** chromophores stand out as favorable candidates for solar cells as compared to other derivatives.

Exciton binding energy (E_b)

The binding energy refers to the minimum energy needed to dissociate an exciton into its individual components (an electron and a hole); this dissociation happens in the excited state generated by photoexcitation[64]. Coulombic forces between holes and electrons are assessed through the evaluation of binding energy. The E_b is influenced by

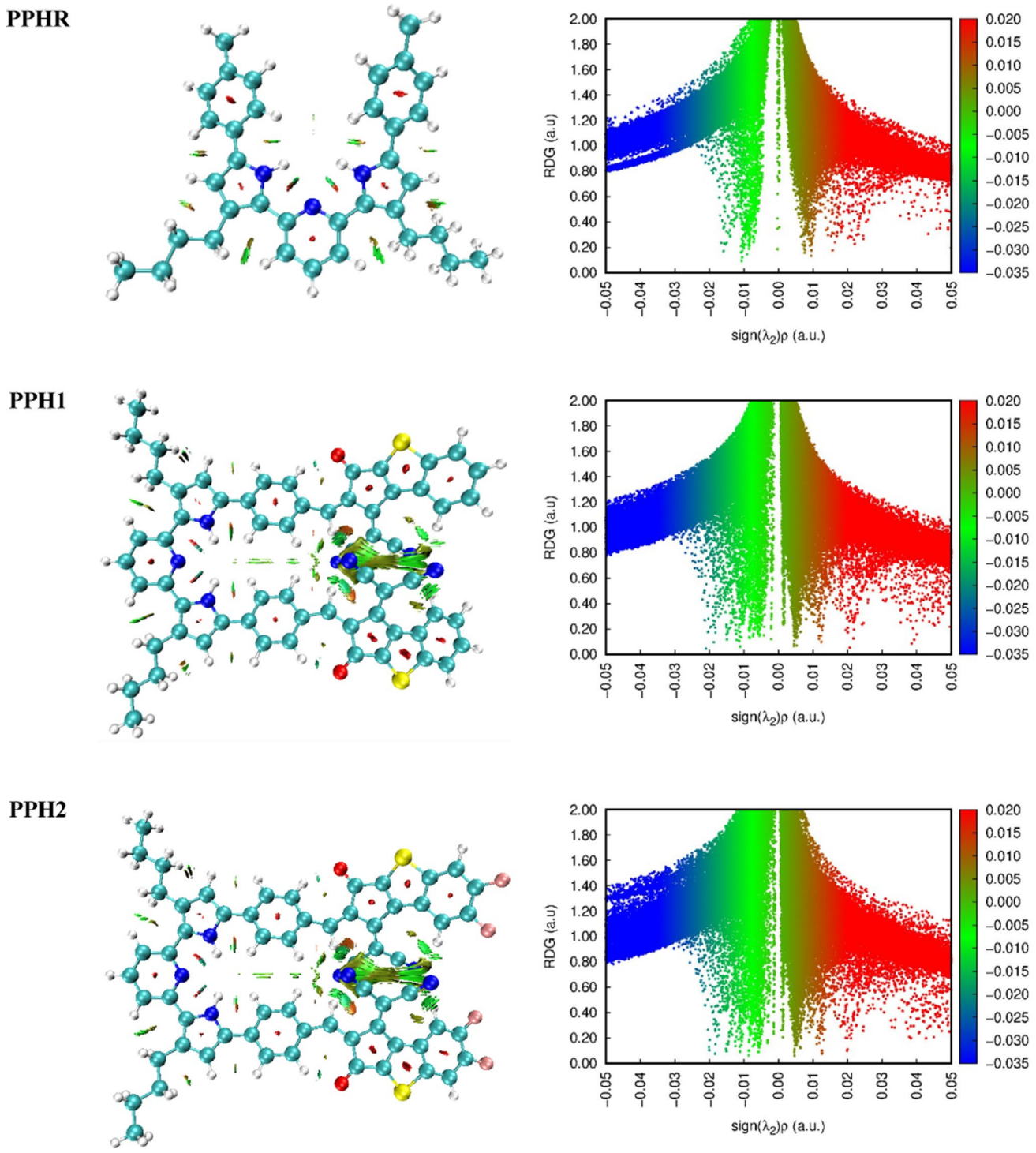

Fig. 6. RDG isosurface densities and scatter plots of investigated compounds.

the acceptor groups at the peripheries of the molecules. Strong electron-withdrawing or highly electronegative groups reduce binding energy by weakening the Coulombic attraction between electrons and holes, as they strongly attract electrons[65]. A reduced binding energy means fewer Columbic forces which in result facilitate efficient exciton splitting into holes and electrons. This enables the charges to migrate to their respective electrodes with greater ease and improves charge mobility in the excited states[66]. The Eq. 1 is used to calculate binding energy values for the investigated compounds[67].

$$E_{\mathrm{b}} = E_{\mathrm{g}} - E_{\mathrm{x}} \tag{1}$$

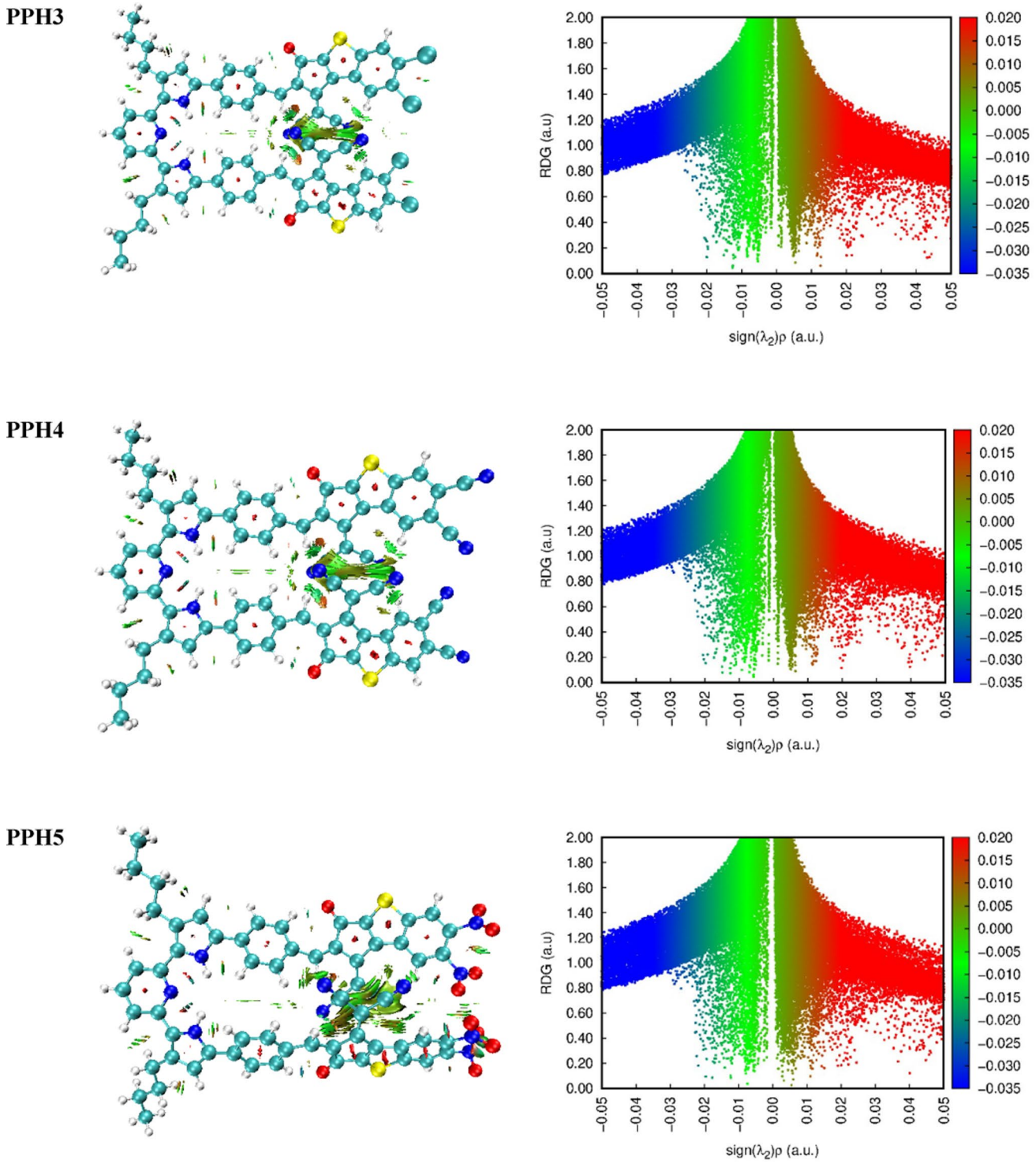

Fig. 6. (continued)

Here, the energy gap is denoted by E_g, and the first excitation energy of an electron from ground state (S_0) to excited state (S_1) is represented by E_x.

Table 3 depicts the calculated E_b values for **PPHR** and **PPH1**-**PPH8** as 0.863, 0.474, 0.469, 0.473, 0.461, 0.487, 0.460, 0.468 and 0.509 *eV*, respectively. Compound (**PPH6**) exhibits the least E_b value (0.460 *eV*) in the selected derivatives, indicating the highest rate of charge dissociation. The E_b in the entitled chromophores follows a declining trend as: **PPHR > PPH8 > PPH5 > PPH1 > PPH3 > PPH2 > PPH7 > PPH4 > PPH6**. Thus, the newly designed compounds show reduced exciton binding energy values as compared to the reference compound, suggesting a higher rate of electron-hole pair dissociation. Reduced exciton binding energies promote effective exciton dissociation into free charge carriers, hence improving charge separation and minimizing the

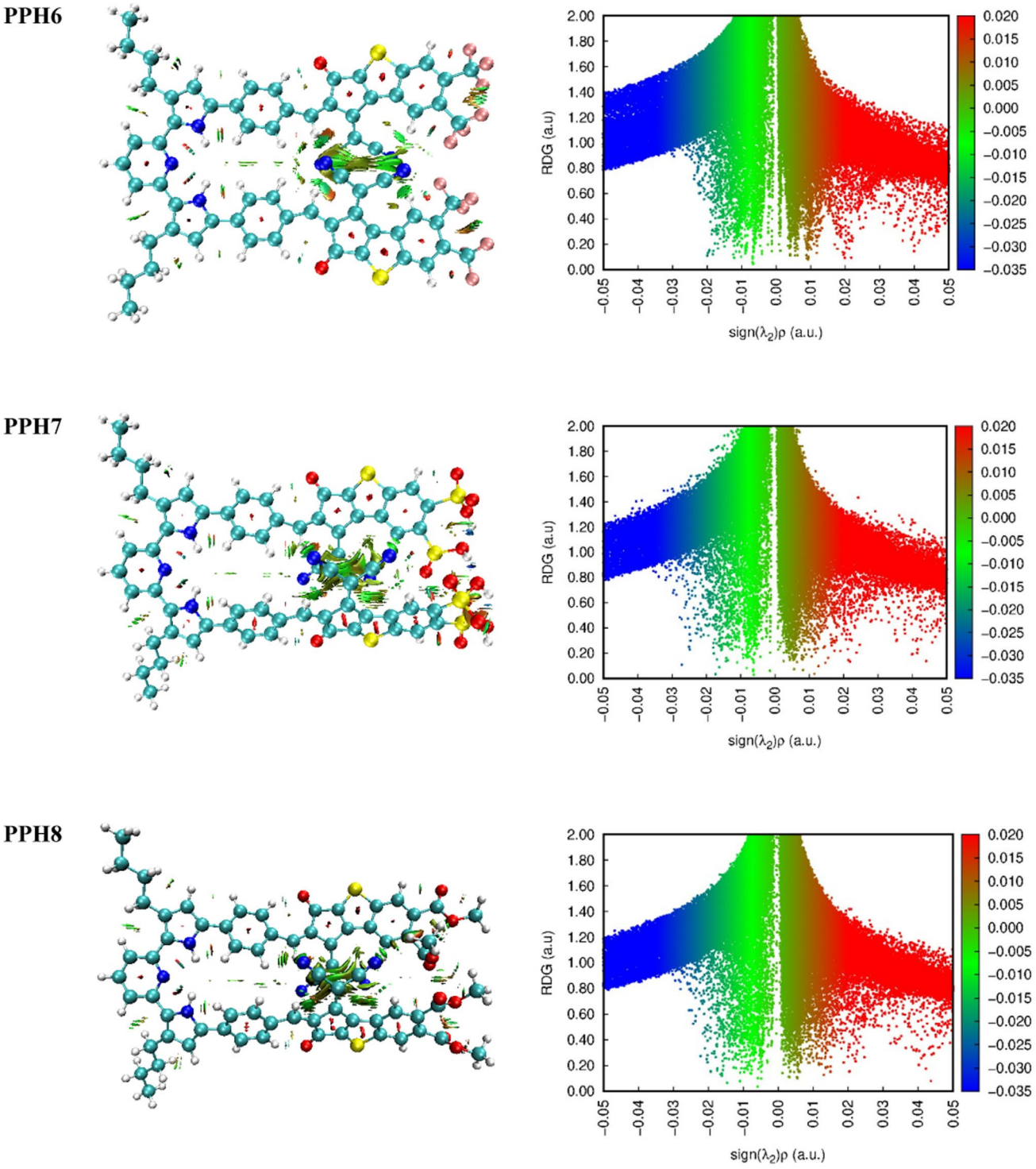

Fig. 6. (continued)

recombination losses. This results in enhanced charge transport properties which are essential for attaining high power conversion efficiency in the organic photovoltaic devices[68].

Concluding this, the findings of E_b are in close harmony with the TDM maps which demonstrate hole-electron localization in accordance with exciton dissociation. Literature shows that lower E_b enhances charge mobility, which in turn increases the short-circuit current density (J_{sc}) as well as improves the power conversion efficiency (PCE) of solar cells[69]. Thus, **PPH6**, **PPH4**, and **PPH7** are likely to demonstrate high charge mobility contributing to the development of more efficient OSCs.

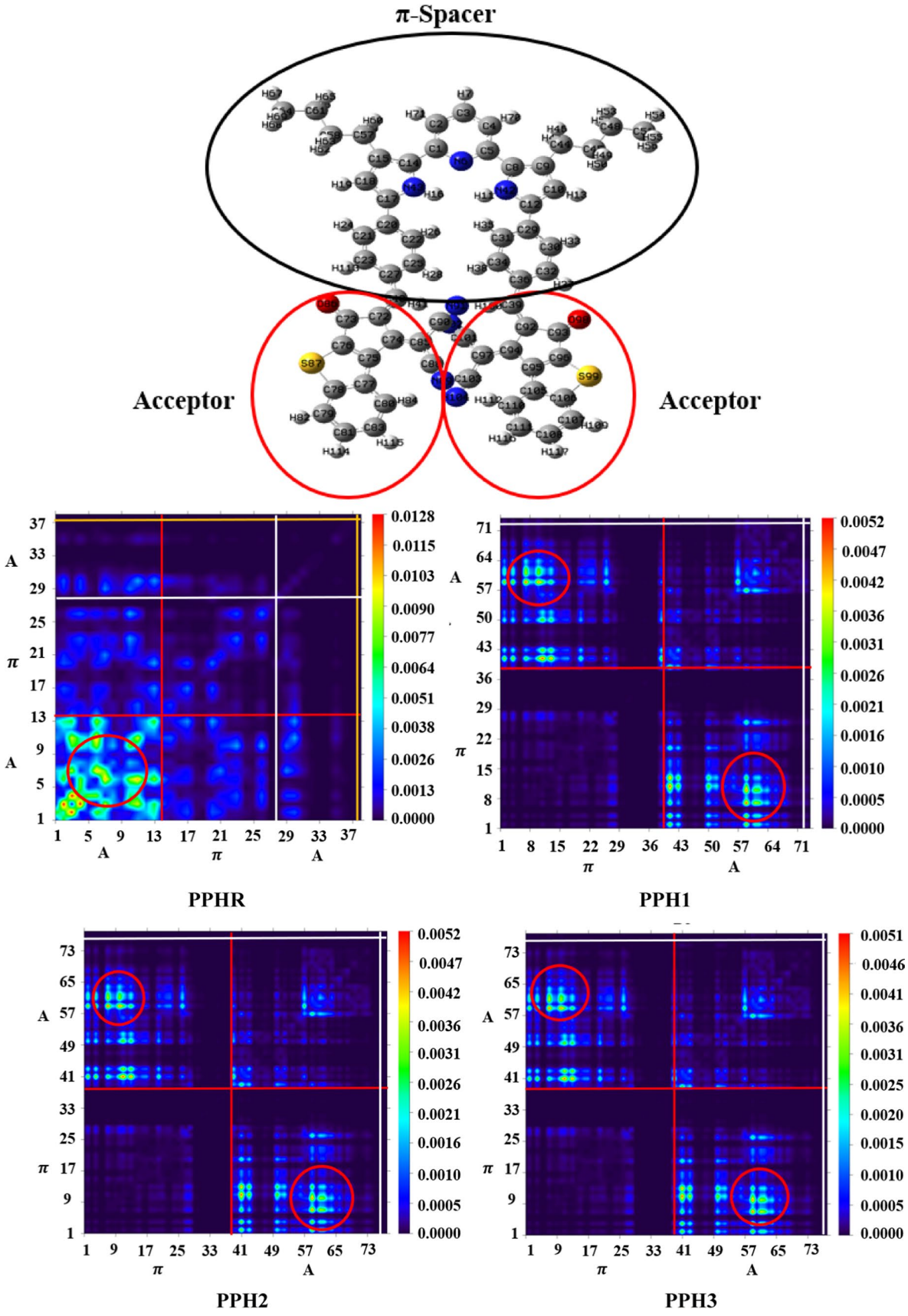

Fig. 7. Transition density matrix diagrams of **PPHR** and **PPH1**- **PPH8** chromophores.

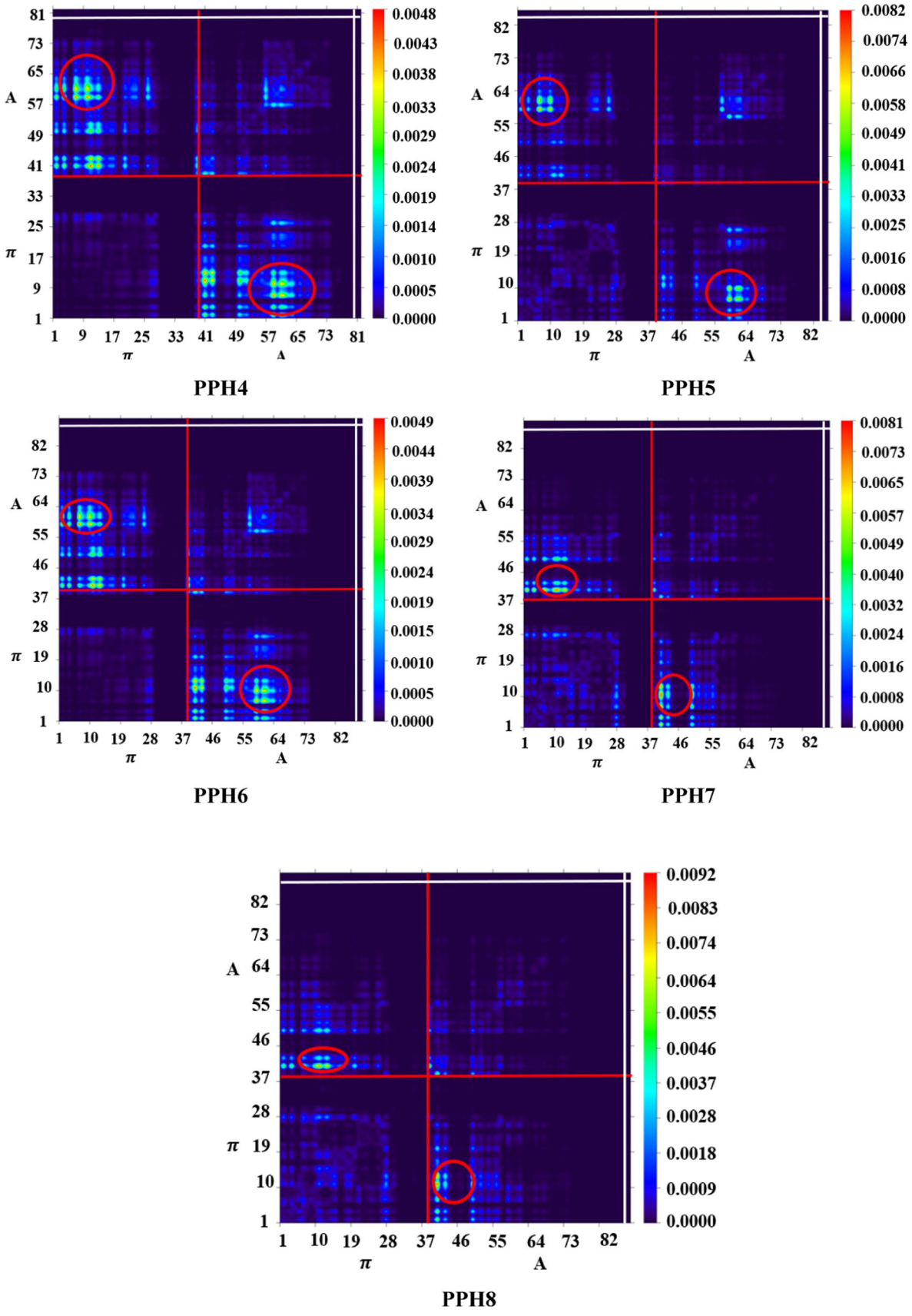

Fig. 7. (continued)

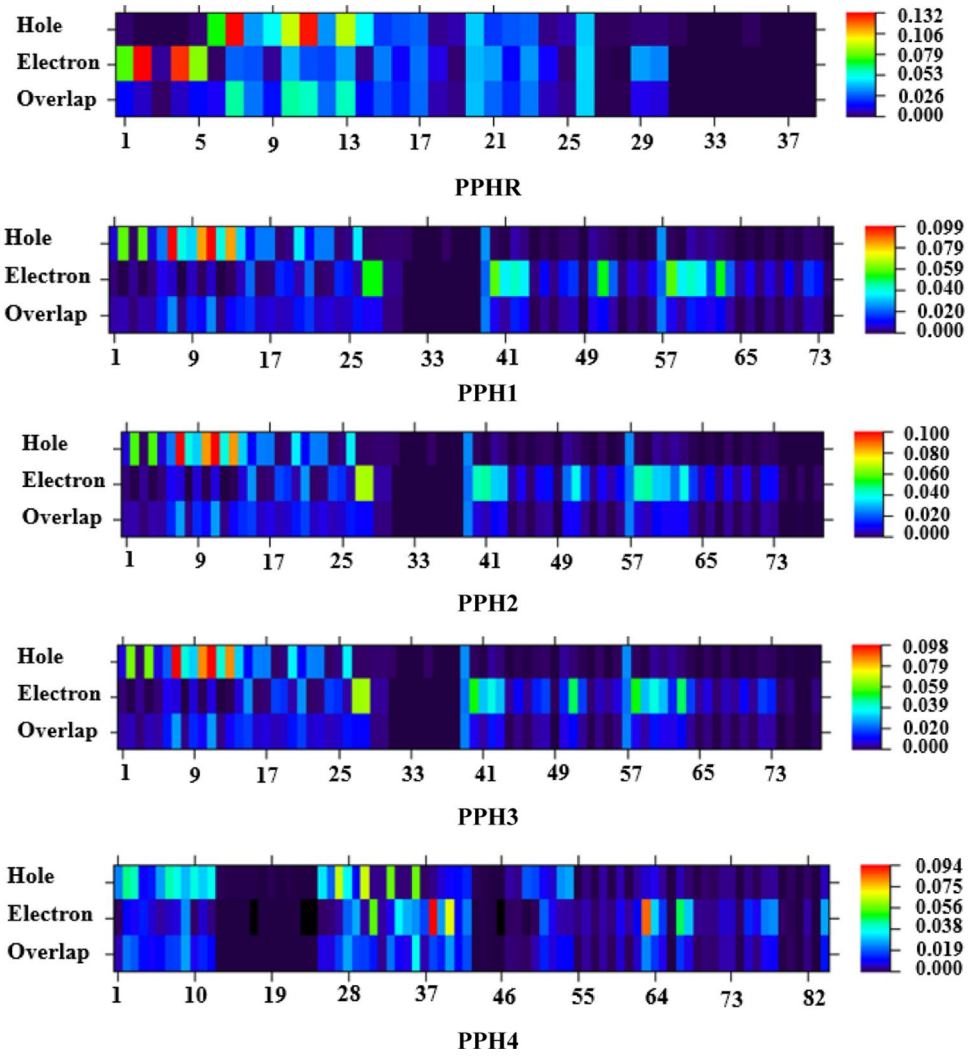

Fig. 8. Electron-hole overlap in all the studied compounds.

Open circuit voltage (V_{oc})

In order to evaluate the performance and maximum working capability of pyridine dipyrrolide material based OSCs, open-circuit voltage analysis is employed. The V_{oc} refers to the maximum voltage in a circuit when no current is flowing[70]. This parameter has a significant impact on the power conversion efficiency of organic solar cells, as they are directly proportional to each other. A high V_{oc}, ideally exceeding 1 V, is crucial for generating highly efficient OSCs. V_{oc} corresponds to the energy difference between the HOMO of the donor material and the LUMO of the acceptor material. Significantly, the value of V_{oc} is highly influenced by both the photo-generated current and saturation voltage[63]. Additionally, the V_{oc} value is influenced by a number of parameters, including the system's temperature, incident light, and the charge-transferring mechanism[71]. Scharber and colleagues formulated a simplified Eq. 2 for calculating V_{oc} in solar cells[72].

$$V_{oc} = \frac{1}{e}(\left|E^{D}_{HOMO}\right| - \left|E^{A}_{LUMO}\right|) - 0.3 \quad (2)$$

In this Equation, E^{D}_{HOMO} represents the HOMO energy of the donor, and E^{A}_{LUMO} denotes the LUMO energy of the acceptor. While "e" representing the elementary charge of the acceptor molecule, and 0.3 acting as an empirical constant derived from the drop factor of voltage. To achieve a higher open-circuit voltage, the energy gap between the HOMO of the donor and the LUMO of the acceptor material must be large, a key factor in enhancing the power conversion efficiency of OSCs. The selection of **$PC_{71}BM$** as a standard acceptor is based on its historical importance and prevalent application as a benchmark acceptor in organic photovoltaics. Its well-defined energy levels, excellent solubility, and proven compatibility with various donor materials render it a suitable reference for comparative V_{oc} assessments[73]. Since a high open-circuit voltage indicates a faster charge transfer rate within the molecule, **$PC_{71}BM$** appears to be the most appropriate acceptor polymer. For this purpose, the HOMO of **PPHR** and **PPH1-PPH8** compounds is coupled with the LUMO of **$PC_{71}BM$** polymer

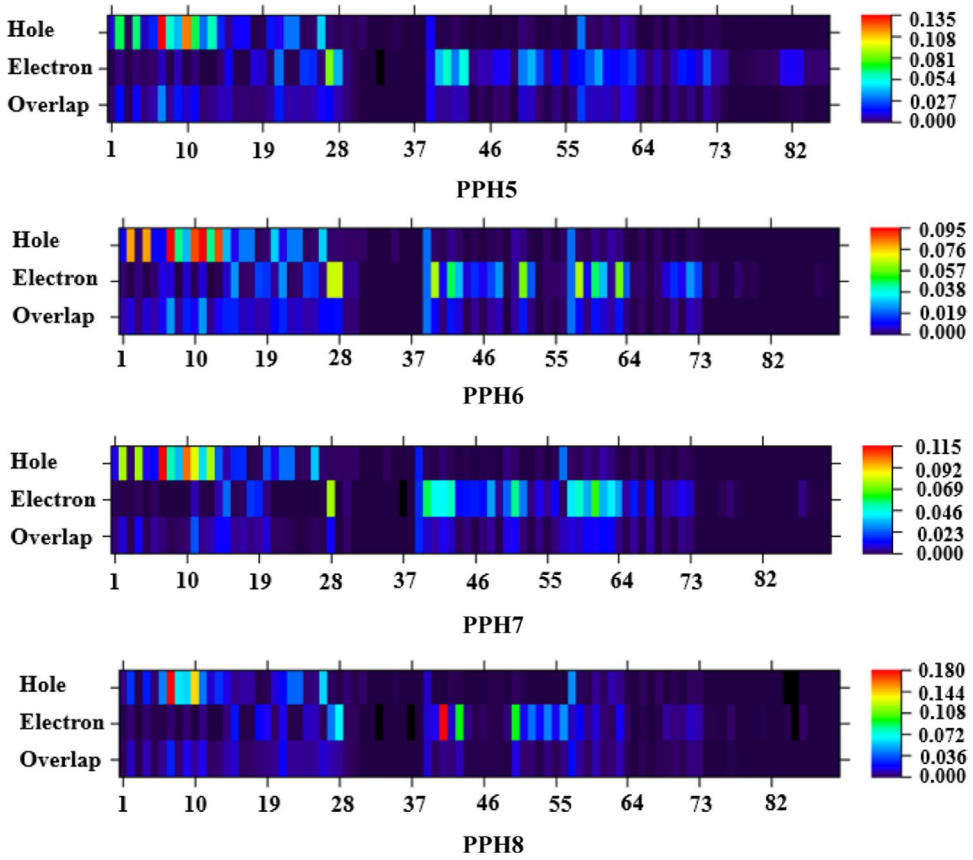

Fig. 8. (continued)

Compounds	E_g	E_x	E_b
PPHR	4.091	3.228	0.863
PPH1	2.677	2.203	0.474
PPH2	2.605	2.136	0.469
PPH3	2.590	2.117	0.473
PPH4	2.468	2.007	0.461
PPH5	2.543	2.056	0.487
PPH6	2.550	2.090	0.460
PPH7	2.491	2.022	0.468
PPH8	2.661	2.152	0.509

Table 3. The calculated values of E_g, E_x, and E_b for the investigated chromophores.

to theoretically determine the V_{oc} of the studied molecules. The LUMO energy level of the **PC_{71}BM** acceptor is observed as −6.05 eV[74]. The pictorial illustration of driving force and V_{oc} is depicted in the Fig. 9.

The energy driving forces are essential for facilitating excitations from the HOMO to the LUMO. A narrower energy gap allows for easy excitation, demanding less energy for the electronic transition between these orbitals. This leads in greater electricity output and a stronger photovoltaic reaction, owing to the surplus energy carried by photons. The observed driving energies for the donor-acceptor complexes (ΔE) are 1.888, 2.313, 2.413, 2.441, 2.675, 2.677, 2.543, 2.621 and 2.439 eV for **PPHR** and **PPH1**-**PPH8**, correspondingly (see Table S15). The declining order of ΔE of all designed systems is found as: **PPH5** > **PPH4** > **PPH7** > **PPH6** > **PPH3** > **PPH8** > **PPH2** > **PPH1** > **PPHR**.

The computed V_{oc} values for **PPHR** and **PPH1**-**PPH8** are 1.588, 2.013, 2.113, 2.141, 2.375, 2.377, 2.243, 2.321, and 2.139 V, respectively. All the studied compounds exhibit higher V_{oc} values compared to the **PPHR**. This indicates that these compounds possess the most significant charge delocalization, attributed to their highly potent acceptor groups incorporated at the terminal ends. In particular, **PPH5** demonstrates the highest V_{oc}, highlighting its superior ability for charge delocalization and power conversion efficiency as compared to other compounds. **PPH5** > **PPH4** > **PPH7** > **PPH6** > **PPH3** > **PPH8** > **PPH2** > **PPH1** > **PPHR** is the declining sequence

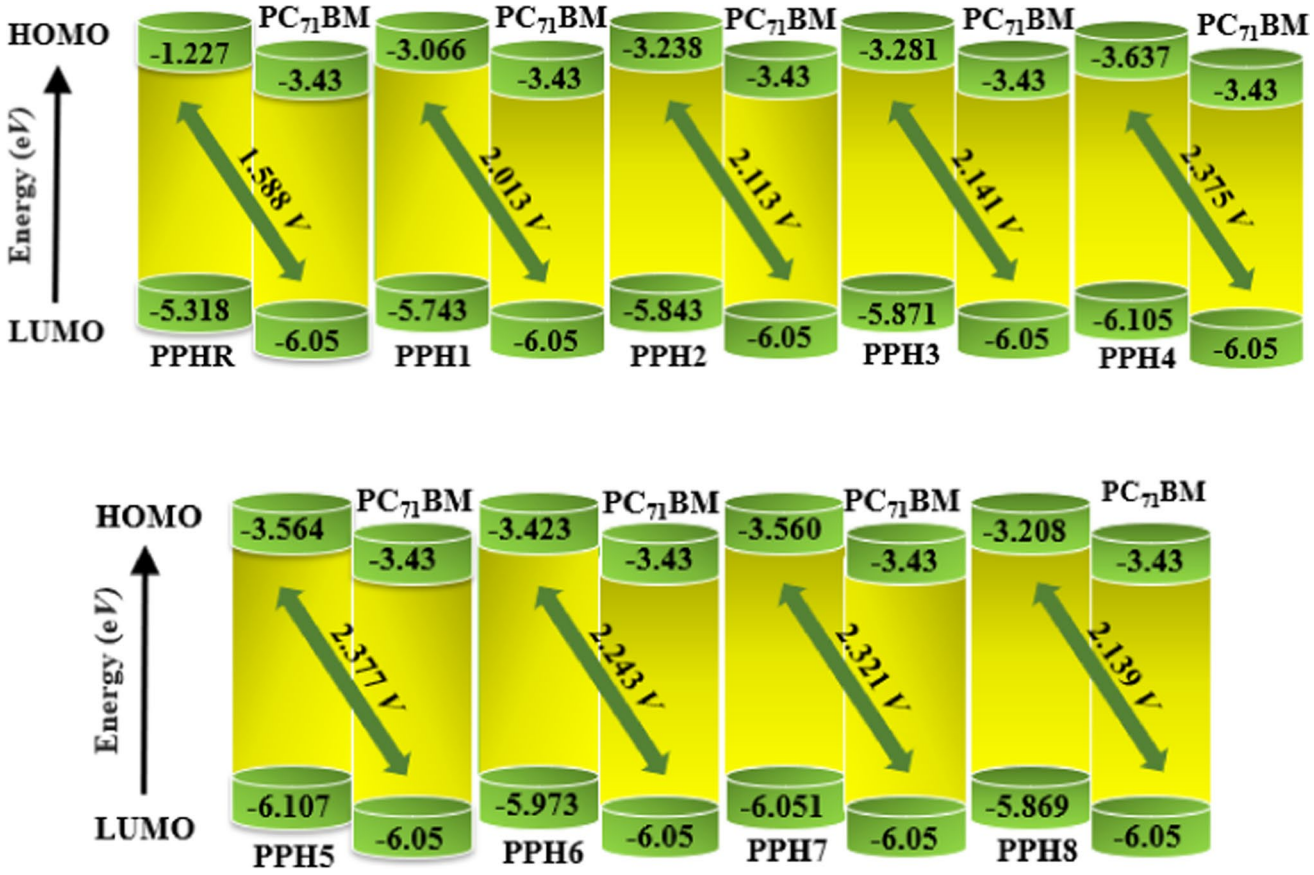

Fig. 9. Graphical representation of V_{oc} of the studied compounds with respect to **$PC_{71}BM$** acceptor.

of V_{oc} for the investigated chromophores. In summary, pyridine dipyrrolide-based chromophores exhibit excellent photovoltaic properties, demonstrating their potential for effective the OSCs materials.

Conclusion

This study illustrates the strategic advantages of end-group modification in improving the optoelectronic characteristics of organic chromophores for use in organic solar cells. Eight novel chromophores (**PPH1–PPH8**) were developed by modifying the terminal acceptor groups of the reference molecule (**PPHR**), demonstrating advantageous characteristics like decreased energy gaps, red-shifted absorbance, effective intramolecular charge transfer, and favorable open-circuit voltages. These findings emphasize the design adaptability of pyridine dipyrrolide-based structures and their significance for next-generation solar materials. In addition to theoretical insights, this research offers a logical chemical framework that can assist experimental chemists in synthesizing good photovoltaic materials. Overall, this work advances the pursuit of sustainable and efficient materials for organic photovoltaics through providing design methodologies especially utilization of benzothiophene based acceptors.

Data availability

All data generated or analyzed during this study are included in this published article and its supplementary information files.

Received: 4 March 2025; Accepted: 7 July 2025
Published online: 16 July 2025

References

1. Brabec, C., Scherf, U. & Dyakonov, V. *Organic Photovoltaics: Materials, Device Physics, and Manufacturing Technologies* (Wiley, 2011).
2. Cao, W. & Xue, J. Recent progress in organic photovoltaics: device architecture and optical design. *Energy Environ. Sci.* **7**, 2123–2144 (2014).
3. Mazzio, K. A. & Luscombe, C. K. The future of organic photovoltaics. *Chem. Soc. Rev.* **44**, 78–90 (2015).
4. Sharif, A., Jabeen, S., Iqbal, S. & Iqbal, J. Tuning the optoelectronic properties of dibenzochrysene (DBC) based small molecules for organic solar cells. *Mater. Sci. Semiconduct. Process.* **127**, 105689 (2021).
5. Ans, M., Iqbal, J., Eliasson, B., saif, M. J. & Ayub, K. Opto-electronic properties of non-fullerene fused-undecacyclic electron acceptors for organic solar cells. *Comput. Mater. Sci.* **159**, 150–159 (2019).

6. Yi, J., Zhang, G., Yu, H. & Yan, H. Advantages, challenges and molecular design of different material types used in organic solar cells. *Nat. Reviews Mater.* **9**, 46–62 (2024).
7. Chen, C. et al. Molecular interaction induced dual fibrils towards organic solar cells with certified efficiency over 20%. *Nat. Commun.* **15**, 6865 (2024).
8. Zhang, C. R. et al. Designing donors and nonfullerene acceptors for organic solar cells assisted by machine learning and Fragment-Based molecular fingerprints. *Solar RRL*. **9**, 2400846 (2025).
9. Amine, M. E. Latest updates of single-junction organic solar cells up to 20% efficiency. *Energies* **16**, 3895 (2023).
10. Moulton, C. J. & Shaw, B. L. Transition metal–carbon bonds. Part XLII. Complexes of nickel, palladium, platinum, rhodium and iridium with the tridentate ligand 2, 6-bis [(di-t-butylphosphino) methyl] phenyl. *J. Chem. Soc. Dalton Trans.* **11**, 1020–1024 (1976).
11. Sorsche, D. et al. Unusual dinitrogen binding and Electron storage in dinuclear Iron complexes. *J. Am. Chem. Soc.* **142**, 8147–8159 (2020).
12. Gowda, A. S., Petersen, J. L. & Milsmann, C. Redox chemistry of Bis(pyrrolyl)pyridine chromium and molybdenum complexes: an experimental and density functional theoretical study. *Inorg. Chem.* **57**, 1919–1934 (2018).
13. Zhang, Y., Petersen, J. L. & Milsmann, C. A luminescent Zirconium(IV) complex as a molecular photosensitizer for visible light photoredox catalysis. *J. Am. Chem. Soc.* **138**, 13115–13118 (2016).
14. Zhang, Y. et al. Delayed fluorescence from a zirconium (IV) photosensitizer with ligand-to-metal charge-transfer excited States. *Nat. Chem.* **12**, 345–352 (2020).
15. Komine, N. et al. Probing the steric and electronic characteristics of a new Bis-Pyrrolide pincer ligand. *Inorg. Chem.* **53**, 1361–1369 (2014).
16. Yadav, S. et al. Phosphine-Free Bis(Pyrrolyl)pyridine based NNN-Pincer Palladium(II) complexes as efficient catalysts for Suzuki-Miyaura Cross-Coupling reactions of Aryl bromides in aqueous medium. *ChemistrySelect* **3**, 9469–9475 (2018).
17. Chang, S. L. et al. Isomerically pure Benzothiophene-Incorporated acceptor: achieving improved V_{oc} and J_{sc} of nonfullerene organic solar cells via end group manipulation. *ACS Appl. Mater. Interfaces*. **11**, 33179–33187 (2019).
18. Manisha et al. Synthesis, characterization, biological activity, DFT, molecular Docking and ADME studies of metal (II) complexes of a bidentate schiff's base (E)-4-chloro-2-((2-hydroxy-3-methoxybenzylidene)amino)benzoic acid. *J. Dispers. Sci. Technol.* 1–14. https://doi.org/10.1080/01932691.2025.2461124 (2025).
19. Gandhi, M., Chavda, V. & Ranga, S. Quinoline schiff bases (QSBs) and their derivatives: emerging trends in antimicrobial agents. *J. Coord. Chem.* **1–34** https://doi.org/10.1080/00958972.2025.2503937 (2025).
20. Ahmedi, S., Tiwari, B., Manzoor, N., Kumar, A. & Jain, P. 3d-Transition metal complexes of a tridentate ligand: synthesis, characterization, Physico-Chemical studies, antimicrobial activity, in Silico molecular Docking and ADME studies. *Chem. Africa* **8**, 1–17 (2025).
21. Cavallo, G., Metrangolo, P., Pilati, T., Resnati, G. & Terraneo, G. Naming interactions from the electrophilic site. *Cryst. Growth. Des.* **14**, 2697–2702 (2014).
22. Concepcion, O. et al. Facile synthesis of diversely functionalized peptoids, spectroscopic characterization, and DFT-Based nonlinear optical exploration. *ACS Omega*. **6**, 26016–26025 (2021).
23. Ali, A. et al. Exploration of structural, electronic and third order nonlinear optical properties of crystalline chalcone systems: monoarylidene and unsymmetrical diarylidene cycloalkanones. *J. Mol. Struct.* **1241**, 130685 (2021).
24. Shafiq, I. et al. Exploration the effect of Selenophene moiety and benzothiophene based acceptors on optical nonlinearity of D–π–A based heterocyclic organic compounds in chloroform solvent: a DFT approach. *J. Mol. Liq.* **393**, 123569 (2024).
25. Khan, I. et al. Palladium-catalyzed synthesis of pyrimidine substituted diaryl ethers through Suzuki Miyaura coupling reactions: experimental and DFT studies. *Optik* **219**, 165285 (2020).
26. Tahir, M. N. et al. Synthesis, single crystal analysis and DFT based computational studies of 2, 4-diamino-5-(4-chlorophenyl)-6-ethylpyrim idin-1-ium 3, 4, 5-trihydroxybenzoate-methanol (DETM). *J. Mol. Struct.* **1180**, 119–126 (2019).
27. Tahir, M. N. et al. Rationalizing the stability and interactions of 2, 4-diamino-5-(4-chlorophenyl)-6-ethylpyrimidin-1-ium 2-hydroxy-3, 5-dinitrobenzoate salt. *J. Mol. Struct.* **1193**, 185–194 (2019).
28. Ma, L. et al. Theoretical study on the effect of end groups and core ring numbers in non-fullerene acceptors for organic solar cells. *Phys. Lett. A*. **518**, 129703 (2024).
29. Frisch, M. J. G. W., Trucks, H. B. & Schlegel GE Scuseria and co-worker. Gaussian. *Inc Wallingford CT* (2009).
30. Bryantsev, V. S., Diallo, M. S., Van Duin, A. C. T. & Goddard, W. A. Evaluation of B3LYP, X3LYP, and M06-Class density functionals for predicting the binding energies of neutral, protonated, and deprotonated water clusters. *J. Chem. Theory Comput.* **5**, 1016–1026 (2009).
31. Kjær, H. & Sauer, S. P. A. Pople style basis sets for the calculation of NMR Spin–Spin coupling constants: the 6-31G-J and 6-311G-J basis sets. *J. Chem. Theory Comput.* **7**, 4070–4076 (2011).
32. Hanwell, M. D. et al. Avogadro: an advanced semantic chemical editor, visualization, and analysis platform. *J. Cheminform*. **4**, 17 (2012).
33. Stevenson, K. J. Review of originpro 8.5. *J. Am. Chem. Soc.* **133**, 5621 (2011).
34. O'Boyle, N. M. & GaussSum Version 2.0. 5, (2007).
35. Lu, T., Chen, F. & Multiwfn A multifunctional wavefunction analyzer. *J. Comput. Chem.* **33**, 580–592 (2012).
36. O'boyle, N. M., Tenderholt, A. L. & Langner, K. M. cclib: A library for package-independent computational chemistry algorithms. *J. Comput. Chem.* **29**, 839–845 (2008).
37. Zhurko, G. A., Zhurko, D. A. & ChemCraft version 1.6. *URL*: (2009). http://www.chemcraftprog.com.
38. Dennington, R., Keith, T. A. & Millam, J. M. GaussView, version 6.0. 16. *Semichem. Inc. Shawnee Mission KS* **13**, (2016).
39. Xie, X., Chen, Z. & Zheng, S. Theoretical exploration of the effects of conjugated side chains on the photoelectric properties of Y6-Based nonfullerene acceptors. *J. Phys. Chem. A*. **129**, 2866–2875 (2025).
40. Abdelaziz, B., Bouazizi, S., Gassoumi, B., Patanè, S. & Ayachi, S. DFT and molecular dynamics study of the optical and electronic properties of nitrobenzofurazan-based molecules for photovoltaic and nonlinear optical applications. *Mater. Chem. Phys.* **332**, 130269 (2025).
41. Zubair, I. et al. Tuning the optoelectronic properties of Indacenodithiophene based derivatives for efficient photovoltaic applications: a DFT approach. *Chem. Phys. Lett.* **793**, 139459 (2022).
42. Sikandar, R. et al. Tuning the optoelectronic properties of oligothienyl silane derivatives and their photovoltaic properties. *J. Mol. Graph. Model.* **106**, 107918 (2021).
43. Fujisawa, J. An unusual mechanism for HOMO–LUMO gap narrowing in a minimal near-IR dye generated by the deprotonation of Bis (dicyanomethylene) Indan. *Chem. Phys. Lett.* **608**, 355–359 (2014).
44. Tsapi, C. T. et al. Exohedral adsorption of N-(4-Methoxybenzylidene) isonicotinohydrazone molecule onto X12N12 nanocages (where X = B and Al) and the effect on its NLO properties by DFT and TD-DFT. *J. Chem.* **2023**, 1–15 (2023).
45. Wang, Y. et al. Recent progress and challenges toward highly stable nonfullerene Acceptor-Based organic solar cells. *Adv. Energy Mater.* **11**, 2003002 (2021).
46. Mahmood, A. et al. Recent progress in porphyrin-based materials for organic solar cells. *J. Mater. Chem. A*. **6**, 16769–16797 (2018).
47. Asogwa, F. C. et al. Experimental and theoretical studies of the influence of alkyl groups on the photovoltaic properties of (E)-6-((2, 3-dihydroxylnaphthalene)diazenyl)-1H-benzoisoquinoline-1,3-dione-based organic solar cell. *J. Mol. Model.* **28**, 245 (2022).

48. Setsoafia, D. D. Y., Ram, K. S., Mehdizadeh-Rad, H., Ompong, D. & Singh, J. Density functional theory simulation of dithienothiophen [3, 2-b]-pyrrolobenzothiadiazole-Based organic solar cells. *Energies* **17**, 313 (2024).
49. Slama, T. et al. Multi-faceted spectroscopic, computational, and nonlinear optical characterization of 2-(pyrrolidin-1-yl)-3,5-dinitropyridine. *J. Mol. Liq.* **418**, 126722 (2025).
50. Zhang, C. R. et al. Modulating the organic photovoltaic properties of non-fullerene acceptors by molecular modification based on Y6: a theoretical study. *Phys. Chem. Chem. Phys.* **25**, 25465–25479 (2023).
51. Nielsen, C. B., Holliday, S., Chen, H. Y., Cryer, S. J. & McCulloch I. Non-fullerene electron acceptors for use in organic solar cells. *Acc. Chem. Res.* **48**, 2803–2812 (2015).
52. Arshad, M. N. et al. Enhancing the photovoltaic properties via incorporation of Selenophene units in organic chromophores with A2-π2-A1-π1-A2 configuration: A DFT-based exploration. *Polymers* **15** (6), 1508 (2023).
53. Siddique, S. A. et al. Efficient tuning of triphenylamine-based donor materials for high-efficiency organic solar cells. *Comput. Theor. Chem.* **1191**, 113045 (2020).
54. Adeel, M. et al. Exploration of CH··· F & CF··· H mediated supramolecular arrangements into fluorinated terphenyls and theoretical prediction of their third-order nonlinear optical response. *RSC Adv.* **11**, 7766–7778 (2021).
55. Contreras-García, J. et al. A benchmark for the non-covalent interaction (NCI) index or… is it really all in the geometry? *Theor. Chem. Acc.* **135**, 1–14 (2016).
56. Mahmood, A., Irfan, A. & Wang, J. L. Molecular level Understanding of the chalcogen atom effect on chalcogen-based polymers through electrostatic potential, non-covalent interactions, excited state behaviour, and radial distribution function. *Polym. Chem.* **13**, 5993–6001 (2022).
57. Khatua, R., Das, B. & Mondal, A. Rational design of non-fullerene acceptors via side-chain and terminal group engineering: a computational study. *Phys. Chem. Chem. Phys.* **25**, 7994–8004 (2023).
58. Mehboob, M. Y. et al. Theoretical modelling of novel indandione-based donor molecules for organic solar cell applications. *J. Phys. Chem. Solids*. **162**, 110508 (2022).
59. Yousaf, I. et al. Isatin-derived non-fullerene acceptors for efficient organic solar cells. *Mater. Sci. Semiconduct. Process.* **121**, 105345 (2021).
60. Shafiq, I. et al. Exploration of photovoltaic behavior of benzodithiophene based non-fullerene chromophores: first theoretical framework for highly efficient photovoltaic parameters. *J. Mater. Res. Technol.* **24**, 1882–1896 (2023).
61. Mahmood, A., HussainTahir, M., Irfan, A., Khalid, B. & Al-Sehemi, A. G. Computational designing of triphenylamine dyes with broad and Red-shifted absorption spectra for Dye-sensitized solar cells using Multi-Thiophene rings in π-Spacer. *Bull. Korean Chem. Soc.* **36**, 2615–2620 (2015).
62. Khalid, M. et al. Promising impact of push–pull configuration into designed octacyclic naphthalene-based organic scaffolds for nonlinear optical amplitudes: A quantum chemical approach. *Sci. Rep.* **13** (1), 20104 (2023).
63. Hussain, R. et al. Designing of silolothiophene-linked triphenylamine-based hole transporting materials for perovskites and donors for organic solar cells-A DFT study. *Sol. Energy*. **253**, 187–198 (2023).
64. Zheng, B. et al. Quantum criticality of excitonic Mott metal-insulator transitions in black phosphorus. *Nat. Commun.* **13**, 7797 (2022).
65. Tang, H. et al. Interface engineering for highly efficient organic solar cells. *Adv. Mater.* **36**, 2212236 (2024).
66. Zhao, Q. et al. Advantageous properties of halide perovskite quantum Dots towards energy-efficient sustainable applications. *Green Energy Environ.* **9** (2023).
67. Khan, M. I. et al. End-capped group modification on cyclopentadithiophene based non-fullerene small molecule acceptors for efficient organic solar cells; a DFT approach. *J. Mol. Graph. Model.* **113**, 108162 (2022).
68. Lin, Y., Li, Y. & Zhan, X. Small molecule semiconductors for high-efficiency organic photovoltaics. *Chem. Soc. Rev.* **41**, 4245 (2012).
69. Abdelaziz, B., Bouazizi, S., Gassoumi, B., Patanè, S. & Ayachi, S. Design and computational analysis of nitrobenzofurazan-based non-fullerene acceptors for organic solar cells: A DFT and molecular dynamics simulation study. *Synth. Met.* **311**, 117846 (2025).
70. Tian, S. et al. Optimization of tail state Urbach energy enables efficient organic solar cells and perovskite/organic tandem solar cells. *Org. Electron.* **113**, 106714 (2023).
71. Rauh, D., Wagenpfahl, A., Deibel, C. & Dyakonov, V. Relation of open circuit voltage to charge carrier density in organic bulk heterojunction solar cells. *Applied Phys. Lett.* **98**, 133301 (2011).
72. Naveed, A. et al. Tuning the optoelectronic properties of benzodithiophene based donor materials and their photovoltaic applications. *Mater. Sci. Semiconduct. Process.* **137**, 106150 (2022).
73. Barreiro-Argüelles, D. et al. Stability study in organic solar cells based on PTB7:PC71BM and the scaling effect of the active layer. *Sol. Energy*. **163**, 510–518 (2018).
74. Wu, Z., Fan, B., Xue, F., Adachi, C. & Ouyang, J. Organic molecules based on dithienyl-2, 1, 3-benzothiadiazole as new donor materials for solution-processed organic photovoltaic cells. *Sol. Energy Mater. Sol. Cells*. **94**, 2230–2237 (2010).

Acknowledgements

The authors thank the Ongoing Research Funding Program (ORG-2025-6), King Saud University, Riyadh, Saudi Arabia.K.C. acknowledges the support from the doctoral research fund of the Affiliated Hospital of Southwest Medical University.

Author contributions

Mashal Khan: Formal analysis; Investigation; Writing - original draft; Visualization.Ayesha Tariq: Data Curation; Writing - review & editing; Formal analysis. Iram Irshad: Formal analysis; Investigation; Writing - review & editing. Muhammad Adnan Asghar: Supervision; Investigation; Resources; software; project administration; Methodology.Tansir Ahamad: Formal analysis; Validation; Visualization.Ke Chen: Data curation; Writing - review & editing; Validation; Visualization.

Declarations

Competing interests

The authors declare no competing interests.

Additional information

Supplementary Information The online version contains supplementary material available at https://doi.org/10.1038/s41598-025-10748-x.

Correspondence and requests for materials should be addressed to M.A.A. or K.C.